### Title

Site-specific regulation of RNA editing with ribose-modified nucleoside analogs in ADAR guide strands




### Journal

Nucleic Acids Research, 52(12)

### ISSN

0305-1048



### Authors

Jauregui-Matos, Victorio

Jacobs, Olivia

Ouye, Randall

et al.



### Publication Date

2024-07-08

### DOI

10.1093/nar/gkae461

Peer reviewed

*Nucleic Acids Research*, 2024, **52**, 6733–6747
https://doi.org/10.1093/nar/gkae461
Advance access publication date: 3 June 2024
**Chemical Biology and Nucleic Acid Chemistry**

# Site-specific regulation of RNA editing with ribose-modified nucleoside analogs in ADAR guide strands

**Victorio Jauregui-Matos [1], Olivia Jacobs [1], Randall Ouye [1], Sukanya Mozumder [1,2], Prince J. Salvador [1], Kyle D. Fink [3] and Peter A. Beal [1,*]**

[1]Department of Chemistry, University of California, Davis, CA, USA
[2]Department of Molecular and Cellular Biology, University of California, Davis, CA, USA
[3]Department of Neurology, Institute for Regenerative Cures and MIND Institute, University of California, Davis Medical Center, Sacramento, CA, USA

*To whom correspondence should be addressed. Email: pabeal@ucdavis.edu

## Abstract

Adenosine Deaminases Acting on RNA (ADARs) are enzymes that catalyze the conversion of adenosine to inosine in RNA duplexes. These enzymes can be harnessed to correct disease-causing G-to-A mutations in the transcriptome because inosine is translated as guanosine. Guide RNAs (gRNAs) can be used to direct the ADAR reaction to specific sites. Chemical modification of ADAR guide strands is required to facilitate delivery, increase metabolic stability, and increase the efficiency and selectivity of the editing reaction. Here, we show the ADAR reaction is highly sensitive to ribose modifications (e.g. 4′-*C*-methylation and Locked Nucleic Acid (LNA) substitution) at specific positions within the guide strand. Our studies were enabled by the synthesis of RNA containing a new, ribose-modified nucleoside analog (4′-*C*-methyladenosine). Importantly, the ADAR reaction is potently inhibited by LNA or 4′-*C*-methylation at different positions in the ADAR guide. While LNA at guide strand positions −1 and −2 block the ADAR reaction, 4′-*C*-methylation only inhibits at the −2 position. These effects are rationalized using high-resolution structures of ADAR-RNA complexes. This work sheds additional light on the mechanism of ADAR deamination and aids in the design of highly selective ADAR guide strands for therapeutic editing using chemically modified RNA.

## Graphical abstract

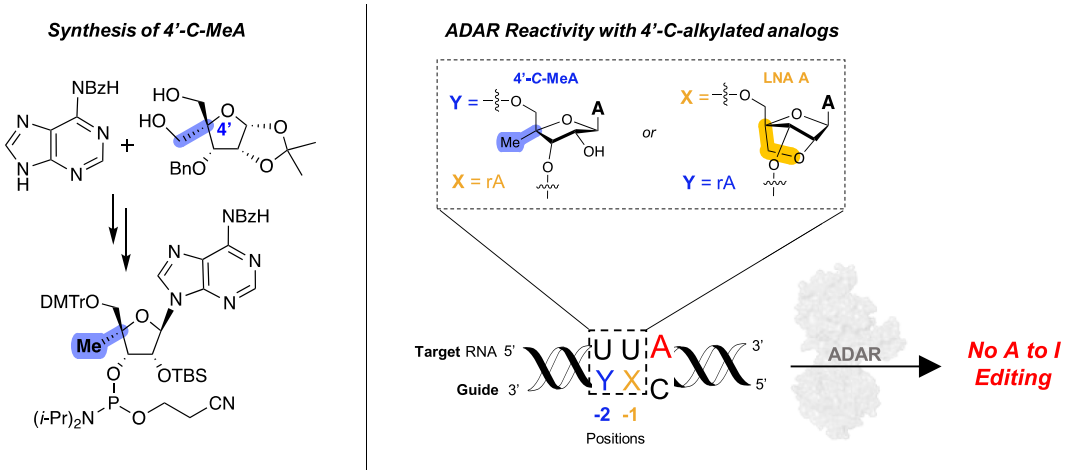


## Introduction

Adenosine (A) to inosine (I) is one of the most prevalent RNA modifications in mammals (1,2). This conversion is catalyzed by a group of enzymes called adenosine deaminases acting on RNA (ADARs) and takes place exclusively in duplex RNA. In humans, ADAR1 and ADAR2 are active adenosine deaminases targeting RNA. Importantly, the A to I reaction can produce codon changes in mRNA because I is read as G during translation (3,4). In addition, since ADARs require duplex structure for activity, their reaction can be directed to specific adenosines in different transcripts using complementary guide strands that form duplexes at the target sites (5). This approach is currently being pursued to develop a new class of therapeutic oligonucleotides that recruit ADARs to correct disease-causing mutations in RNA (6). Chemical modifications are required for these ADAR-guiding oligonucleotides to

**Received:** December 10, 2023. **Revised:** April 12, 2024. **Editorial Decision:** May 11, 2024. **Accepted:** May 26, 2024

facilitate delivery, increase metabolic stability, and increase the efficiency and selectivity of the ADAR reaction (7–11). Identifying and characterizing ADAR guide strand modification patterns that lead to highly efficient and selective editing at different therapeutically relevant target sites is an ongoing effort by several laboratories in academics and industry (7–10). In earlier work, our group showed that placing a single locked nucleic acid (LNA) monomer at a position opposite an editing site's 5′ nearest neighbor nucleotide resulted in dramatically reduced editing at the targeted adenosine (10). Here, we probe the effect of LNA modification at other positions in ADAR guide strands. Furthermore, we describe efforts to define the mechanism by which ADARs are inhibited by LNA modification at specific positions in the guide strand. These efforts were facilitated by the synthesis of RNA oligonucleotides bearing 4′-*C*-methylated nucleoside analogs designed to probe the steric effect of a small 4′-alkyl substituent without the conformational restriction of the 4′-*C*, 2′-oxymethylene linkage found in the LNA monomers. Importantly, while LNA modification potently inhibited target site editing at two adjacent sites in the ADAR guide strand (-1 and -2), this effect is seen for the 4′-*C* Me modification only at the −2 position. The ability of a 4′-*C*-methylated nucleoside to retain editing at the -1 site but not at the −2 site provides a novel method to block bystander editing in 5′-AA target sequences. Finally, these results are rationalized considering the different effects of steric and conformational flexibility at different positions in ADAR guide strands.

## Materials and methods

### Synthesis of 4′-C-methyladenosine (4′-C-MeA) phosphoramidite

$N^6$-Benzoyl-2′-*O*-acetyl-3′-*O*-benzyl-4′-*C*-methyl-5′-*O*-tert-butyldiphenylsilyladenosine, **2**. To a suspension of $N^6$-benzoyladenine (2.07 g, 8.66 mmol, 2 eq.) and an anomeric mixture of the protected and methylated sugar 1 (2.5 g, 4.33 mmol) in anhydrous $CH_2Cl_2$ (31 ml) at 0°C was added tin tetrachloride in one portion (0.5 ml, 4.33 mmol, 1 eq.) under an argon atmosphere. After 16 h of stirring at room temperature, the reaction was quenched with 2 ml of saturated $NaHCO_3$ dropwise at 0°C. The organic layer was diluted with 200 ml of $CH_2Cl_2$ and extracted twice with 100 ml of a saturated solution of $NaHCO_3$. The combined organics were dried over $Na_2SO_4$, filtered, and reduced under pressure to afford a white and oily precipitate. The crude mixture was chromatographed with silica gel with 0.3% MeOH in $CHCl_3$ ($R_f$ = 0.22, 3% MeOH in $CH_2Cl_2$) to afford 2 as a light colorless foam in 63% yield (2.05 g). $^1$H NMR (400 MHz, $CDCl_3$) δ 9.11 (s, 1H), 8.70 (s, 1H), 8.20 (s, 1H), 8.04 (d, $J$ = 7.1 Hz, 2H), 7.67–7.31 (m, 20H), 6.28 (d, $J$ = 5.1 Hz, 1H), 5.98 (t, $J$ = 5.5 Hz, 1H), 4.69 (d, $J$ = 5.7 Hz, 1H), 4.62 (q, $J$ = 38.9 Hz, 2H), 3.88 (d, $J$ = 11.0 Hz, 1H), 3.59 (d, $J$ = 11.0 Hz, 1H), 2.09 (s, 3H), 1.38 (s, 3H), 1.08 (s, 9H). $^{13}$C NMR (101 MHz, $CDCl_3$) δ 206.95, 169.90, 152.72, 151.55, 149.56, 141.79, 137.55, 135.65, 135.53, 133.73, 132.77, 132.71, 132.60, 129.96, 129.92, 128.86, 128.48, 128.04, 127.92, 127.88, 127.84, 123.37, 87.58, 86.01, 75.01, 74.25, 68.06, 30.94, 26.95, 20.72, 19.24, 18.53. Orbitrap-HRMS calculated for $C_{43}H_{45}N_5O_6Si$ $[M + H]^+$ 756.31 *m/z*, found 756.3234 *m/z*.

$N^6$-Benzoyl-3′-*O*-benzyl-4′-*C*-methyl-5′-*O*-(*tert*-butyldiphenylsilyl)adenosine, **3**. To a solution of **2** (0.214 g, 0.283 mmol) in 11 ml of MeOH was added $K_2CO_3$ (0.473 g, 3.42 mmol, 12 eq.) at 0°C and stirred at this temperature for 1.5 h. After completion of the reaction, the mixture was neutralized with 10 ml of aqueous 10% HCl (v/v). The aqueous phase was separated and extracted three times with 10 ml of $CH_2Cl_2$. The combined organics were dried over $Na_2SO_4$, filtered, and reduced under pressure to afford a colorless syrup. The crude mixture was purified by silica gel chromatography with a gradient of 1.75 to 2.25% MeOH in dichloromethane ($R_f$ = 0.43, 4% MeOH in $CH_2Cl_2$) to afford **3** as a colorless foam in 88% yield (178 mg). $^1$H NMR (300 MHz, $CDCl_3$) δ 9.18 (s, 1H), 8.68 (s, 1H), 8.08 (s, 1H), 8.03 (d, $J$ = 6.9 Hz, 1H), 7.71–7.25 (m, 20H), 6.01 (d, $J$ = 5.8 Hz, 1H), 4.92 (t, $J$ = 5.8 Hz, 1H), 4.74 (q, 2H), 4.41 (d, $J$ = 5.8 Hz, 1H), 3.86 (d, $J$ = 10.8 Hz, 1H), 3.88 (s, 1H), 3.58 (d, $J$ = 10.8 Hz, 1H), 1.44 (s, 3H), 1.08 (s, 9H). $^{13}$C NMR (76 MHz, $CDCl_3$) δ 152.47, 151.36, 149.56, 141.86, 137.13, 135.63, 135.53, 133.70, 132.77, 132.71, 132.60, 130.03, 128.84, 128.73, 128.40, 128.15, 127.94, 127.90, 127.88, 123.27, 89.00, 87.52, 79.34, 77.51, 77.08, 76.66, 74.68, 74.51, 68.46, 26.95, 19.27, 19.01. Orbitrap-HRMS calculated for $C_{41}H_{43}N_5O_5Si$ $[M-H]^-$ 712.29 *m/z*, found 712.2974 *m/z*.

$N^6$-Benzoyl-3′-*O*-benzyl-4′-*C*-methyladenosine, **4**. Compound **3** (0.178 g, 0.249 mmol) was co-evaporated twice with anhydrous THF. Subsequently, the silyl-protected nucleoside was dissolved in an anhydrous 1M TBAF solution in THF (0.5 ml) and stirred for 24 h at room temperature under an argon atmosphere. After complete conversion of the starting material, the mixture was reduced to an orange-colored oil and chromatographed with silica gel with a 2–3% MeOH in $CH_2Cl_2$ eluent to afford **4** as a white solid in 79% (93 mg) ($R_f$ = 0.35, 5% MeOH in $CH_2Cl_2$). $^1$H NMR (300 MHz, $CDCl_3$) δ 9.43 (s, 1H), 8.67 (s, 1H), 7.96 (d, 2H), 7.75 (s, 1H), 7.58–7.25 (m, 8H), 6.14 (s, 1H), 5.73 (d, $J$ = 7.6 Hz, 1H), 5.13 (t, $J$ = 6.6 Hz, 1H), 4.75 (q, 2H), 4.30 (d, $J$ = 5.6 Hz, 2H), 3.89–3.69 (m, 2H), 3.58 (d, $J$ = 12.5 Hz, 1H), 1.86 (q, 1H), 1.36 (s, 3H). $^{13}$C NMR (76 MHz, $CDCl_3$) δ 164.59, 151.94, 150.12, 143.19, 137.27, 133.22, 132.84, 128.75, 128.70, 128.41, 128.25, 127.86, 123.92, 91.14, 89.11, 80.78, 75.18, 74.29, 69.02, 67.99, 25.62, 18.67. Orbitrap-HRMS calculated for $C_{25}H_{25}N_5O_5$ $[M + H]^+$ 476.19 m/z, found 476.1935 *m/z*.

$N^6$-Benzoyl-4′-*C*-methyladenosine, **5**. Debenzylation procedure was adapted from Zhou *et al.* (11) **4** (0.230 g, 0.484 mmol) was co-evaporated 3× with anhydrous dichloromethane and dried overnight under high vacuum with a stir bar. The 3′ benzylated nucleoside was then dissolved in 20 ml of anhydrous dichloromethane and stirred 5 min at −78°C under an argon atmosphere, followed by the dropwise addition of 1 M $BCl_3$ in $CH_2Cl_2$ (3.6 ml, 3.6 mmol, 7.5 eq.) over 10 min. After stirring for 4 h at the same temperature, the reaction was quenched with 16 ml of MeOH followed by 3.2 g of $NaHCO_3$. The mixture was left stirring for 4 h at room temperature. The insoluble solid was then filtered through a silica gel pad (2.8 g) and washed with 49 ml of 2:1 DCM:MeOH. The filtrate was evaporated to dryness and chromatographed with silica gel using a 3–8% gradient MeOH in $CH_2Cl_2$ to afford **5** as a white solid in 41% yield (75 mg) $R_f$ = 0.15 (10% MeOH in $CH_2Cl_2$). $^1$H NMR

(400 MHz, DMSO) δ 11.10 (s, 1H), 8.72 (d, $J$ = 14.0 Hz, 2H), 8.09–8.03 (m, 2H), 7.65 (t, $J$ = 7.3 Hz, 1H), 7.55 (t, $J$ = 7.6 Hz, 2H), 6.02 (d, $J$ = 7.2 Hz, 1H), 5.46 (d, $J$ = 6.3 Hz, 1H), 5.30 (t, $J$ = 5.8 Hz, 1H), 5.21 (d, $J$ = 4.7 Hz, 1H), 4.91 (d, $J$ = 6.5 Hz, 1H), 4.11 (t, $J$ = 4.6 Hz, 1H), 3.57 (dd, $J$ = 11.6, 4.8 Hz, 1H), 3.44–3.35 (m, 3H), 1.20 (s, 3H). $^{13}$C NMR (101 MHz, DMSO) δ 166.39, 152.72, 152.00, 143.75, 134.17, 132.80, 128.98, 128.90, 126.40, 87.94, 87.89, 87.36, 74.44, 72.27, 67.39, 40.60, 40.39, 40.18, 39.97, 39.76, 39.55, 39.34, 19.30. Orbitrap-HRMS calculated for $C_{18}H_{19}N_5O_5$ [M + H]$^+$ 386.14 *m/z*, found 386.1475 *m/z*.

*5′-O-(4,4′*-Dimethoxytrityl)-*N*$^6$-benzoyl-4′-*C*-methyladenosine, **6.** After co-evaporating **5** (0.118 g, 0.300 mmol) 3× with anhydrous pyridine (3 × 2 ml) and drying it overnight under high vacuum, the nucleoside was dissolved with distilled and anhydrous pyridine (2.0 ml). DMTr-Cl (0.124 g, 0.367 mmol, 1.2 eq.) was added in one portion to the solution, followed by the catalytic addition of 4-dimethylaminopyridine (DMAP) (1.7 mg, 0.014 mmol, 0.046 eq.). The solution was stirred for 24 h under argon and at room temperature and quenched with 1 ml of MeOH. All the volatiles were evaporated and the resulting crude was diluted with 30 ml of $CH_2Cl_2$, washed 1× with 5% aqueous $NaHCO_3$ (10 ml), 1× with brine (10 ml), dried over $Na_2SO_4$ and filtered. The crude was purified via silica gel chromatography (base washed with 1% TEA) with a gradient of 0–2.75% MeOH in $CH_2Cl_2$ to give **6** as a light yellow foam in 70% yield (144 mg). $R_f$ = 0.18 (4% MeOH in $CH_2Cl_2$). $^1$H NMR (300 MHz, $CDCl_3$) δ 9.18 (s, 1H), 8.71 (s, 1H), 8.22 (s, 1H), 8.03 (d, $J$ = 7.5 Hz, 2H), 7.58 (dt, $J$ = 28.4, 7.4 Hz, 3H), 7.37–7.09 (m, 10H), 6.74 (d, $J$ = 8.3 Hz, 4H), 6.04 (d, $J$ = 6.2 Hz, 1H), 5.93 (s, 1H), 5.01 (t, $J$ = 5.8 Hz, 1H), 4.34 (d, $J$ = 5.2 Hz, 1H), 3.76 (s, 6H), 3.28 (d, $J$ = 10.0 Hz, 1H), 3.14 (d, $J$ = 10.0 Hz, 1H), 1.43 (s, 3H), 0.89 (d, $J$ = 9.2 Hz, 1H). $^{13}$C NMR (76 MHz, $CDCl_3$) δ 158.51, 152.10, 150.93, 149.61, 144.33, 141.55, 135.38, 135.28, 133.50, 132.96, 130.00, 129.16, 128.94, 127.97, 127.90, 127.84, 126.92, 123.11, 113.13, 90.46, 89.13, 86.71, 77.47, 77.05, 76.63, 76.18, 73.71, 68.47, 55.23, 29.73, 18.98. Orbitrap-HRMS calculated for $C_{39}H_{37}N_5O_7$ [M + H]$^+$ 688.27 *m/z*, found 688.2744 *m/z*.

*5′-O-(4,4′*-Dimethoxytrityl)-2′-*O*-(*tert*-butyldimethylsilyl)-*N*$^6$-benzoyl-4′-*C*-methyladenosine, **7**. Prior to silylation, **6** was co-evaporated 3x with anhydrous pyridine and dried under high vacuum overnight. To a solution of **6** (0.124 g, 0.180 mmol) in anhydrous pyridine and THF (2.25 ml, 1:1) was added silver nitrate (0.035 g, 0.200 mmol, 1.16 eq.) under an argon atmosphere at 0°C. After stirring for 5 min, TBS-Cl (0.030 g, 0.200 mmol, 1.16 eq.) was added in one portion at the same temperature. The reaction was allowed to stir overnight at room temperature. After the starting material was consumed, the reaction was diluted with 10 ml of ethyl acetate and filtered. The filtrate was collected and evaporated to a yellow oil, diluted with 10 ml of $CH_2Cl_2$, and washed once with 5% aqueous $NaHCO_3$. After drying and filtering the organic phase with $Na_2SO_4$, the crude was chromatographed with a base-washed (0.5% TEA) silica gel column with a gradient of 0–40% ethyl acetate in *n*-hexanes ($R_f$ = 0.41, 8:3 *n*-hexane:EtOAc). Purification afforded **7** as a colorless foam in 64% yield (92 mg). $^1$H NMR (300 MHz, $CD_2Cl_2$) δ 9.16 (s, 1H), 8.68 (s, 1H), 8.18 (s, 1H), 8.03 (d, $J$ = 7.6 Hz, 2H), 7.73–7.15 (m, 12H), 6.98–6.79 (m, 4H), 6.09 (d, $J$ = 5.8 Hz, 1H), 5.19 (t, $J$ = 5.5 Hz, 1H), 4.42 (t, $J$ = 3.6 Hz, 1H), 3.82 (s, 6H), 3.45 (d, $J$ = 9.9 Hz, 1H), 3.25 (d, $J$ = 9.9 Hz, 1H), 2.87 (d, $J$ = 3.6 Hz, 1H), 2.04 (s, 1H), 1.44 (s, 3H), 0.88 (s, 9H), 0.01 (s, 3H), -0.17 (s, 3H). $^{29}$Si NMR (60 MHz, $CD_2Cl_2$) δ 24.61. $^{13}$C NMR (76 MHz, $CD_2Cl_2$) δ 164.42, 158.70, 152.43, 151.61, 149.65, 144.82, 142.14, 135.65, 135.60, 134.06, 132.63, 130.14, 130.11, 128.82, 128.12, 127.90, 127.76, 126.89, 123.49, 113.15, 88.16, 86.83, 86.58, 75.80, 72.63, 68.01, 55.21, 29.69, 25.31, 18.86, 17.73, -5.33, -5.44. Orbitrap-HRMS calculated for $C_{45}H_{51}N_5O_7Si$ [M + H]$^+$ 802.36 m/z, found 802.3658 *m/z*.

*5′-O-(4,4′*-Dimethoxytrityl)-3′-*O*-[(2-cyanoethoxy)(*N,N*-diisopropylamino)phosphino]-2′-*O*-(*tert*-butyldimethylsilyl)-*N*$^6$-benzoyl-4′-*C*-methyladenosine, **8.** Compound 7 was co-evaporated 3× with anhydrous $CH_2Cl_2$ (8 ml) and dried overnight under $P_2O_5$ and high vacuum. To a solution of 7 (0.092 g, 0.114 mmol), DMAP (2.7 mg, 0.0228 mmol, 0.2 eq.), distilled over $CaH_2$*N,N*-diisopropylethylamine (60 μl, 0.342 mmol, 3 eq.), and 0.45 ml of anhydrous $CH_2Cl_2$ was added 2-cyanoethyl *N,N*-diisopropylchlorophosphoramidite (50 μl, 0.230 mmol, 2 eq.) under an argon atmosphere. The reaction was allowed to stir overnight at room temperature. The reaction was quenched with 0.1 ml of MeOH and further diluted with dichloromethane. The organic phase was then washed with 5% aqueous $NaHCO_3$ once, dried over $Na_2SO_4$ and filtered to afford a yellow-orange oil. The residue was purified over a 0.5% TEA-washed silica gel column with a gradient of 30–45% ethyl acetate in *n*-hexanes to furnish the phosphoramidite 8 as a colorless foam in 77% yield (88 mg) (diastereomers of 8, $R_f$ = 0.64, 0.52 in 54% ethyl acetate in *n*-hexanes). $^{31}$P NMR (122 MHz, $CD_2Cl_2$) δ 150.19, 149.87. Orbitrap-HRMS calculated for $C_{54}H_{68}N_7O_8PSi$ [M + H]$^+$ 1002.47 *m/z*, found 1002.4713 *m/z*.

## Solid-phase oligonucleotide synthesis and purification

All oligonucleotides were synthesized in 0.2 μmol scale based on the phosphoramidite chemistry and standard DNA/RNA reagents and cycles. DMTr-Off and 2′-*O*-TBDMSi protecting strategy was employed for all RNA oligonucleotide synthesis. The coupling time for all phosphoramidites was between 3 and 10 min. For incorporation of the 4′-*C*-MeA phosphoramidite, an extended coupling time of 45 min was used and was dissolved with a 3:1 mixture of MeCN:DCM to 0.1 M(16). Before its incorporation, the purified phosphoramidite was co-evaporated 3x with anhydrous DCM, filtered using syringe filter and was dried under high vacuum overnight over $P_2O_5$. Coupling efficiency of the 4′-*C*-MeA was measured by means of the conductivity released by the trityl cation during detritylation of the growing strand with 3% trichloroacetic acid in $CH_2Cl_2$ and was comparable with commercially available phosphoramidites detritylations. Post synthesis, columns were dried for 2 h under high vacuum. Cleavage from the solid support and deprotection of the nucleobases were accomplished using a fresh aliquot of ammonium hydroxide in ethanol at 55°C for 12 h (1 ml of 28–30% $NH_4OH$/EtOH in 0.5 ml EtOH). After cleavage, the solid support was allowed to cool to room temperature and centrifuged for 5 min at 13 000 × g. The supernatants were collected and lyophilized. 2′-*O*-silyl ether deprotection was done using 250 μl of anhydrous 1M tetrabutylammonium fluoride (TBAF) in THF for 24 h at room temperature. Crude oligonucleotides were desalted by

precipitation with the addition of 1 ml of 1-butanol and 50 μl of 3 M NaOAc and cooled for 2 h at −70°C. The solution was centrifuged at 13 000 × g for 30 min, supernatants were removed, and the pellets were washed twice with cold 95% ethanol.

The oligonucleotides were purified by loading a 1:1 mixture of 10–20 nmol of crude RNA to 80% formamide in 1× Tris-borate EDTA (TBE) and 1mM EDTA into a denaturing polyacrylamide gel. Depending on their size, oligonucleotides were loaded into different acrylamide matrices with different percentages and electrophoresed in 1× TBE. After visualization by UV shadowing on glass-backed silica gel plates, gel bands were excised, crushed, and soaked overnight at 4°C in 0.5 ml of 0.5 M $NH_4OAc$ and 0.1 mM EDTA. Gel particles were removed from the extracted RNA by filtering the suspension for 5 min, 13 000 × g on 0.2 μm cellulose sterile membrane filter tubes (Corning). The oligonucleotides were precipitated from a solution of 75% EtOH at − 70°C for 2 h. The oligonucleotides were then pelleted from the solution by centrifugation (13 000 × g for 30 min), with the supernatant being discarded. The pellets were lyophilized to dryness, resuspended in nuclease-free water, and quantified by absorbance at 260 nm. Oligonucleotide mass was confirmed by MALDI-TOF (Supplementary Information, Table S2).

## Target RNA synthesis

The gene fragment of the corresponding human MECP2, mouse IDUA, human SRC, modified IDUA and MECP2, and human PPP2R5D were purchased from Integrated DNA Technologies. These were amplified with New England BioLabs (NEB) Q5 Hot Start high-fidelity DNA polymerase and purified by extraction from 1% agarose gels. Target RNA was synthesized with NEB's HiScribe T7 RNA polymerase according to the protocol. The target RNAs were purified by 8% denaturing polyacrylamide gel electrophoresis.

## Hybridization of guide and target RNA

The target and guide RNA were combined in a 1:10 ratio of target:guide to a final concentration of 180 nM of hybrids in 1× TE and 100 mM NaCl. This solution was heated to 95°C for 5 min then it was allowed to cool to room temperature for 2 h.

## ADAR1 p110 overexpression and purification

Human ADAR1 p110 (UniProtKB P55265-5) with a C-terminal intein fusion protein with chitin binding domain (CBD) was overexpressed in *S. cerevisiae* BCY123 as previously described (12). Human ADAR1 p110 was purified by lysing cells in 20 mM Tris−HCl pH 8.0, 5% (v/v) glycerol, 750 mM NaCl, 50 mM imidazole, 1 mM tris(2-carboxyethyl)phosphine-HCl (TCEP-HCl), 50 $\mu$M $ZnCl_2$ and EDTA-free Protease Inhibitor using a microfluidizer. The lysate was centrifuged at 39 000 × g for 45 min at 4°C. The clarified lysate was passed over an equilibrated chitin binding column using gravity flow and was incubated for 2 h at 4°C for binding. The chitin column was then washed with 10 column volumes (CV) of lysis buffer and subsequently, the column was quickly washed with 5 bed volumes of the cleavage buffer (20 mM Tris−HCl pH 8.0, 5% (v/v) glycerol, 350 mM NaCl, 50 mM imidazole, 50 mM DTT and 50 μM $ZnCl_2$. To ensure cleavage of the CBD domain, the resin was incubated in 2 CVs of cleavage buffer overnight at room temperature for 18 h. The protein was eluted by washing columns with an additional 5 CVs of cleavage buffer. Finally, the eluted target protein was pooled, concentrated to 0.3 mg/ml, and then dialyzed against a storage buffer containing 20 mM Tris−HCl pH 8.0, 20% (v/v) glycerol, 350 mM NaCl, 50 mM imidazole, 1 mM TCEP-HCl. Protein concentration was determined by running the sample alongside bovine serum albumin (BSA) standards in a sodium dodecyl sulfate-PAGE (SDS-PAGE) gel followed by SYPRO Orange (Invitrogen) staining. The protein was stored at −80°C in aliquots for further use.

## ADAR2 wild-type (WT) and ADAR2 E488Q overexpression and purification

ADAR2 wild-type and E488Q mutant overexpression and purification were performed as previously described (13)

## In vitro deamination reactions and Sanger sequencing

For ADAR2 WT and ADAR2 E488Q deaminations, hybridized target and guide RNA were diluted to 5 nM in 1× ADAR2 reaction buffer (15 mM Tris–HCl pH 7.5, 3% glycerol, 60 mM KCl, 1.5 mM EDTA, 0.003% Nonidet *P*-40 and 3 mM $MgCl_2$), 0.5 mM dithiothreitol (DTT), 160 units/ml RNAse inhibitor, 1 μg/ml yeast tRNA and 15 nM ADAR2 protein. The reactions were conducted at 30°C. For two time points reactions analysis, as well as for kinetic analysis (1, 3, 5, 10, 15, 30, 60 min), aliquots of 8 μl were quenched with 190 μl of 95°C heated nuclease-free water for 5 min. Single turnover conditions were achieved by reacting duplex RNA with excess enzyme (three-fold or greater excess, depending on ADAR isoform). For ADAR1 p110 deaminations, hybridized target and guide RNA were diluted to 15 nM in 1× ADAR1p110 reaction buffer (15 mM Tris–HCl pH 7.5, 3% glycerol, 26 mM KCl, 40 mM potassium glutamate, 1.5 mM EDTA, 0.003% Nonidet *P*-40 and 4% glycerol), 0.5 mM DTT, 160 units/ml RNAse inhibitor, 1 μg/ml yeast tRNA and 150 nM ADAR1 p110. Due to the lower enzymatic activity of overexpressed and purified ADAR1 p110, a higher concentration of molar ratio of ADAR1 than ADAR2 was used to optimize deamination reactions. The reactions were conducted the same way as ADAR2. A 5 μl aliquot of each time point quench solution was reverse transcribed with Access Reverse Transcription (RT) Polymerase Chain Reaction (RT-PCR) system purchased from Promega. DNA was cleaned and concentrated using Zymo's purification kit and protocol. For Sanger sequencing with Azenta Life Sciences, purified DNA was diluted to 0.66 ng/μl in 1.6 μM of forward or reverse sequencing primer. Sanger sequencing traces were observed with SnapGene Viewer and statistical analysis along with nonlinear fits were conducted with Microsoft Excel and GraphPad Prism. The editing level for the corresponding zero time point was subtracted from each data point as background subtraction.

## Oligonucleotide metabolic stability assay

A 60 μM stock solution of oligonucleotide was made in IDT Nuclease-Free Buffer (30 mM HEPES, pH 7.5; 100 mM potassium acetate). In a 50 μl reaction volume, the oligonucleotide sample was diluted to a final concentration of 8 μM with Dulbecco's Phosphate Buffer Saline (DPBS, Gibco 14190144) in 80% human serum (Millipore Sigma H4522). Each reaction was incubated at 37 °C and 5 uL aliquots were taken out at

0, 2, 4, 6, 8, 10, 12 and 16 h and combined with 5 ul of 80% formamide in 1X TBE and 1 mM EDTA, vortexed and immediately stored at −80°C. Each aliquoted time point containing 40 pmol of oligonucleotide was loaded into a 15% denaturing Novex TBE Gels (Invitrogen, EC62752BOX or EC63152BOX) and electrophoresed at 200 V for 60 min in 1× TBE. The gel was then stained in SYBR Gold Nucleic Acid Gel Stain (Invitrogen S11494) for 30 min and imaged on the GelDoc Go Imaging System (Bio-Rad) under SYBR Gold settings on a UV/Stain-free tray. The densitometry of RNA bands was determined using Image Lab and plotted by a function of time using GraphPad Prism.

### Oligonucleotide melting temperature assay

Melting temperature analysis of oligonucleotides was performed as previously described (14).

### Directed editing on endogenous β-actin transcript in HEK293T cells

Procedure was performed as previously described (15).

## Results

### Inhibition of the ADAR reaction by LNA substitution is highly position-dependent

Previously, we showed that an LNA monomer located at the −1 position on an ADAR guide strand inhibited target editing and that strategic positioning of LNA could block unwanted bystander editing when the off-target was placed at least 6 nucleotides away from the target(14). Since LNA modifications in RNA therapeutics could be useful for enhancing target RNA binding affinity and resistance to nuclease degradation, we tested how ADAR responded to LNA modification at other positions in the guide RNA (16). We allowed ADAR2 to react with an RNA duplex bearing the sequence present in the c-Src mRNA. c-Src is a protein kinase frequently overexpressed in cancers (17). Specifically, we targeted for RNA editing the K295 codon (5′-A**A**A-3′). Editing of the central adenosine will convert this to an arginine codon resulting in a K295R mutation that renders the oncogenic protein kinase inactive (18). The sequence surrounding the target site is 5′-AUCA**A**AA-3′, where the target adenosine is directly flanked by two potential bystander editing sites (Figure 1A) with two additional bystander sites nearby. We first determined the percent editing by human ADAR2 at 60 min for the desired target and the four bystander sites employing an unmodified guide RNA as a control for comparison with the LNA-containing guide RNAs (Figure 1B). We then modified each sugar independently starting from the −4 position to the +3 position of the guide relative to the target adenosine and measured the percent editing for the target and bystander sites (Figure 1C-I). A schematic of the numbering of positions relative to the target A in the guide RNA is shown in Figure 1A, including the 'orphan' position, which is the base on the guide opposite to the target adenosine. Without LNA modifications, we observed significant editing of bystander adenosines four nucleotides and one nucleotide 5′ and one nucleotide 3′ of the target A. However, certain patterns of inhibition were observed depending on whether the LNA monomer was placed in the guide 5′ or 3′ of the orphan position. For instance, LNA placement 3′ of the orphan position at positions -4 and -3 in the guide RNA reduced by > 50% or blocked editing entirely at the bystander sites, while also reducing editing at the target site by 43% and 46%, respectively (Figure 1C and 1F). Moreover, when the LNA monomers were placed closer to the target site in positions -2 and -1, editing at the target site and bystander sites decreased by > 95% for each site (Figure 1D-E). A very different editing profile was observed when LNA monomers were positioned 5′ of the orphan nucleotide. When LNA monomers were placed +1, +2 and + 3 in the guide RNA, either no inhibition (+2 and + 3) or less than two-fold reduction (+1) was observed. Yet, sites opposite the 3′ base flanking the LNA monomer or directly across it showed reduced or inhibited editing (Figure 1I).

### High-resolution structures reveal possible origin of LNA inhibition of the ADAR reaction

Intrigued by the potent inhibitory effect of LNA monomers at the −1 and −2 positions of a guide RNA, we sought to understand the mechanistic origin of this phenomenon. The available high-resolution structures of ADAR2 bound to duplex RNA show that the ribose 4′ carbon (4′-C) at the −1 position is in proximity (4.4 Å) to the γ and δ carbons of isoleucine 491 (I491) (Figure 2) (19). This residue lies on a loop involved in stabilizing the flipped-out conformation required for adenosine deamination by ADARs (Figure 2C) (20,21). Furthermore, these structures also show this nucleotide adopts an unusual conformation with a DNA-like C2'-*endo* sugar pucker, a high anti glycosidic bond angle, and a disruption of base stacking (Figure 2E) (10). Likewise, these structures also reveal that the 4′-C of the −2 nucleotide in the guide RNA approaches even more closely (3.7 Å) the side chain of proline 492, a highly conserved amino acid in the ADAR family of enzymes while retaining an RNA-like C3'-*endo* sugar pucker (Figure 2D and F) (22).

These observations suggested that inhibition by the substitution of the −1 and −2 nucleotides in the guide RNA with an LNA monomer could result from steric or conformational effects (or both). In the case of each of the −1 and −2 LNA nucleotides, one can predict a steric clash between the side chains of I491 and P492 with the 4′-C-2′-oxymethylene linkage present in the minor groove at an LNA sugar. Considering that the −1 nucleotide undergoes an RNA-to-DNA sugar pucker conversion, inhibition when LNAs are placed at this position could arise from the restricted/locked conformation. To distinguish the possible origins of the inhibitory effect of LNA substitution in ADAR guide strands (i.e. restricted conformation or steric clash), we compared LNA substitution to two nucleoside analogs with different sugar methylation sites. We envisioned these analogs arising from cleaving either the bond between 2′-O and 6′-C to afford 4′-C-methyladenosine (4′-C-MeA) or cleavage of the 4′-C and 6′-C bond to furnish 2′-O-methyladenosine (2′-O-MeA) (Figure 3). Each of these analogs retain the atoms present in LNA A, but lack the conformational constraint imposed by the 4′-C to 2′-O bridge. Thus, if the steric demand of the additional methylene present in LNA A (compared to rA) was responsible for the inhibitory effect, at least one of these two analogs would be expected to inhibit the ADAR reaction when placed at the corresponding position in the guide strand. However, if each were well tolerated by ADAR, the LNA effect on conformational flexibility would be the more likely origin of inhibition. Since ADAR's preferred 5′ nearest neighbor nucleotide is U or A (i.e. 5′-U**A** or 5′-A**A**), the −1 nucleotide in a guide RNA targeting these

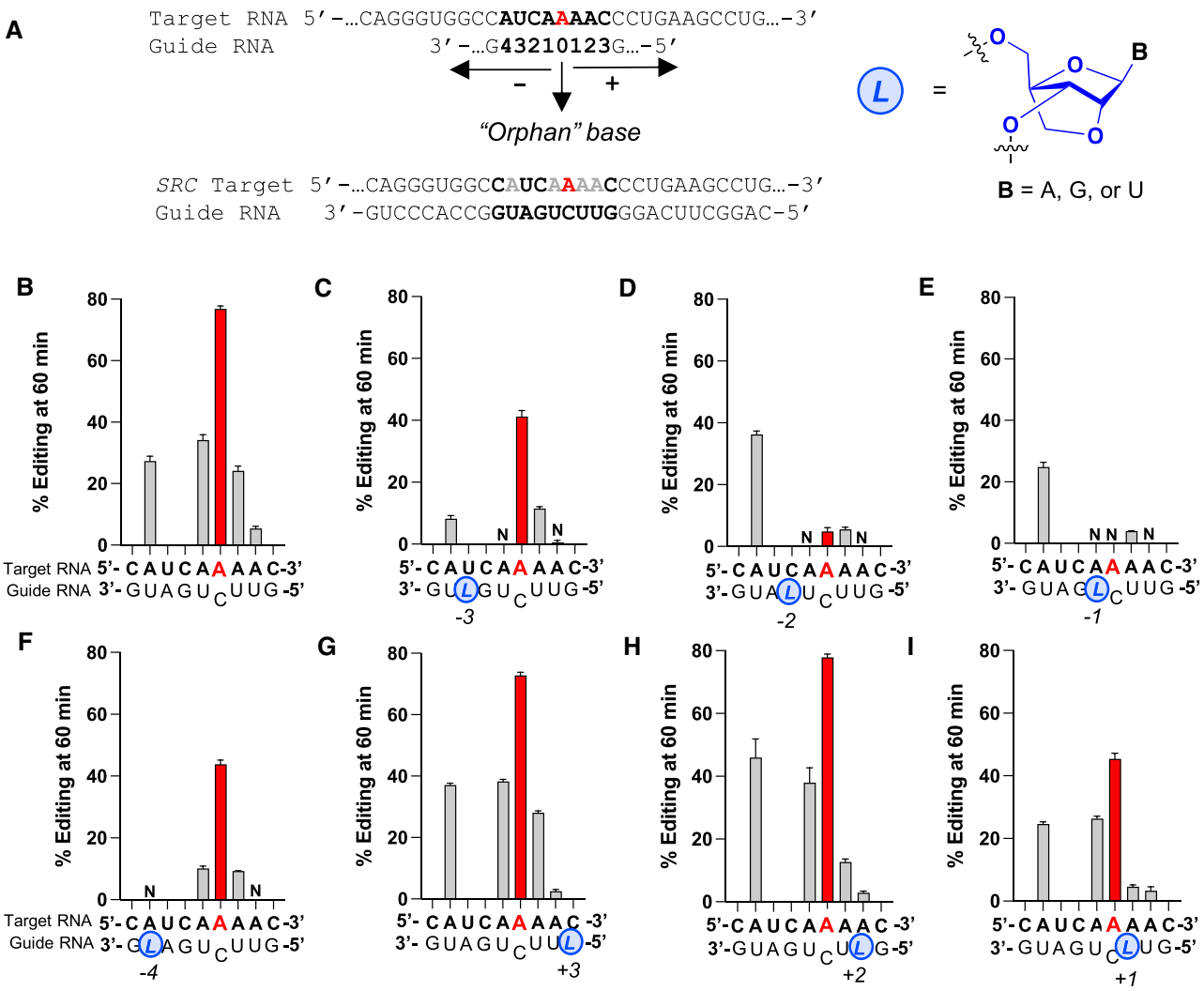


**Figure 1.** Site-specific LNA modification can reduce or block editing at various off-target sites by ADAR2 on the *SRC* transcript. (**A**) Left top: schematic of target:guide strand duplex indicating nomenclature and numbering scheme used in this work; bottom left: Target RNA and guide RNA hybrid construct; red A: adenosine target; grey: bystander sites; bold: fragment studied for the LNA modifications. Right: structure of LNA in blue. (**B**) Editing yield at 60 min with no LNA modification. Red bars indicate editing for target A; off-target sites are displayed in light grey bars. (**C–I**) Editing yield at 60 min for different guide oligonucleotides bearing LNA (blue and *italics L*) at different sites on the guide RNA (−3, −2, −1, −4, +3, +2 and +1, respectively). Reactions for each time point were carried out with a ratio of 5:50 nM of RNA hybrid to ADAR2 WT. Error bars represent the standard deviation of three technical replicates. N: No detected editing.

sequences is uridine or adenosine. Yet, in this project, we tested sugar analogs of adenosine for studies of mostly 5′-U**A** targets. In addition to the 2′-*O*-MeA, LNA A and 4′-*C*-MeA, we also tested the unlocked nucleic acid version of adenosine (UNA A). Since UNA A is highly flexible, results with this analog could determine to what extent flexibility is beneficial at the -1 position (23).

## 4′-*C*-Methyladenosine phosphoramidite and RNA synthesis

To incorporate each of these modifications into RNA, their corresponding phosphoramidites were needed. However, the 4′-*C*-MeA phosphoramidite had not been previously reported. Waga *et al.* developed a synthetic strategy to incorporate 4′-*C*-alkyl substituents into free ribonucleosides to test for effects on HIV replication (24,25). Furthermore, Koizumi and Kano synthesized 4′-*C*-aminoalkyl uridine modified RNA and tested for effects on siRNA delivery in RNA interference (26,27). Lastly, Guo et al. synthesized a 4′-*C*-methyluridine phosphoramidite and modified RNA to understand the effects of 4′-*C*-alkylation on ribose conformation during base-catalyzed RNA cleavage via internal transesterification (28). Here, we used a seven-step synthesis to furnish the 4′-*C*-MeA phosphoramidite starting from the previously synthesized 4′-α-*C*-methylribose **1** in reasonable yields (Scheme 1) (29,30). Initially, regioselective $N^9$ ribosylation with $N^6$-benzoyladenine and tin tetrachloride ($SnCl_4$) afforded the protected adenosine analog **2**. The desired regioisomer was identified by heteronuclear multiple bond correlation (HMBC), heteronuclear single bond correlation (HSQC), and homonuclear correlation (COSY) NMR experiments (Supplementary Information, Figure S1A). In these experiments, the $N^7$ analog displayed an interaction between the glycosyl anomeric hydrogen and $C^5$ and $C^8$ of the purine, while for the $N^9$ analog, the anomeric hydrogen interacts with carbons $C^4$ and $C^8$ (31). In addition, the selective formation of the β-ribonucleoside is supported by Höfler and Vorbrüggen's mechanistic explanation of

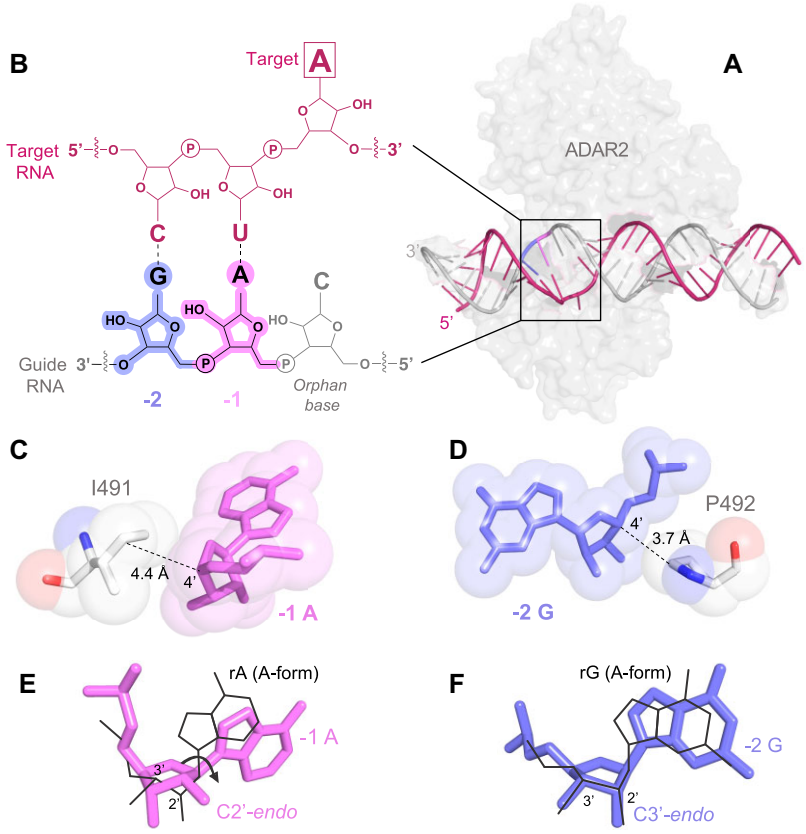


**Figure 2.** Structure of hADAR2-R2D E488Q bound to the GLI1 32 bp RNA at 2.8 Å resolution (19). (**A**) View of the structure perpendicular to the dsRNA helical axis, the pink and slate blue region shows the kink in the guide RNA and the widening of the major groove opposite the editing site induced by ADAR2. The warm pink shows the target RNA and the light grey the guide RNA. (**B**) Schematic of target and guide RNA hybrid for ADAR editing in a 5′-UA-3′ sequence context indicating nomenclature and numbering scheme used in this work. −1 position highlighted in pink and −2 in blue. (**C**) Space filling model of the −1 nucleotide 4′-*C* closely approaching the γ and δ carbons of I491 in ADAR's flipping loop. (**D**) Space filling model of the −2 nucleotide 4′-*C* closely approaching P492's side chain. (**E**) The −1 A (pink) adopts a C2′-*endo* sugar pucker with a high anti glycosidic bond angle (χ = −90.6°) compared to an ideal A-form nucleotide (black). (**F**) The −2 G (slate blue) adopts an RNA canonical C3′-*endo* sugar pucker (black).

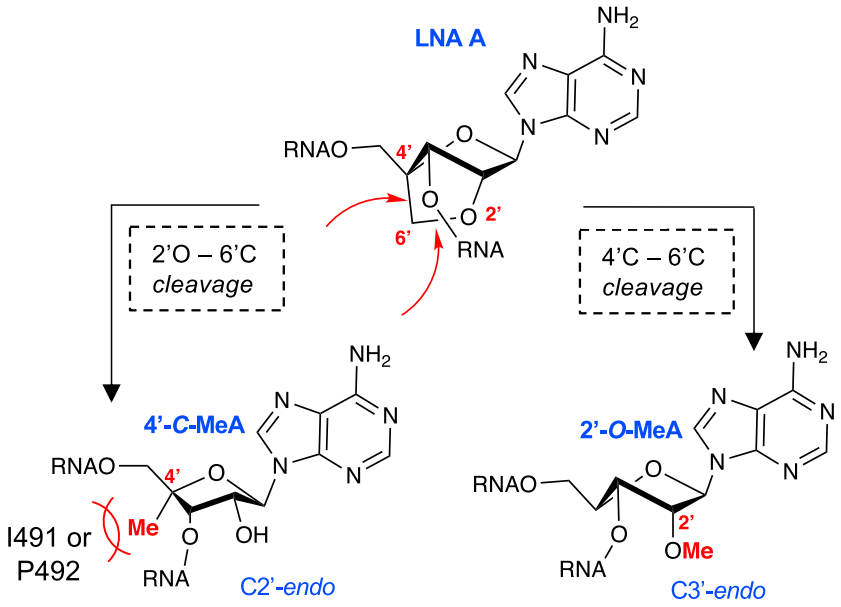


**Figure 3.** Proposed structures of the possible methyl groups rearranged from the 2′-*C*-4′-*C*-oxymethylene linkage cleavage of LNA at the −1 position. LNA is fixed to an RNA C3′-*endo* sugar pucker conformation. Right: 2′-*O*-Me A; Left: 4′-*C*-MeA and proposed steric clash with I491 or P492. 4′-*C*-Me A expected to adopt a DNA-like C2′-*endo* sugar pucker conformation.

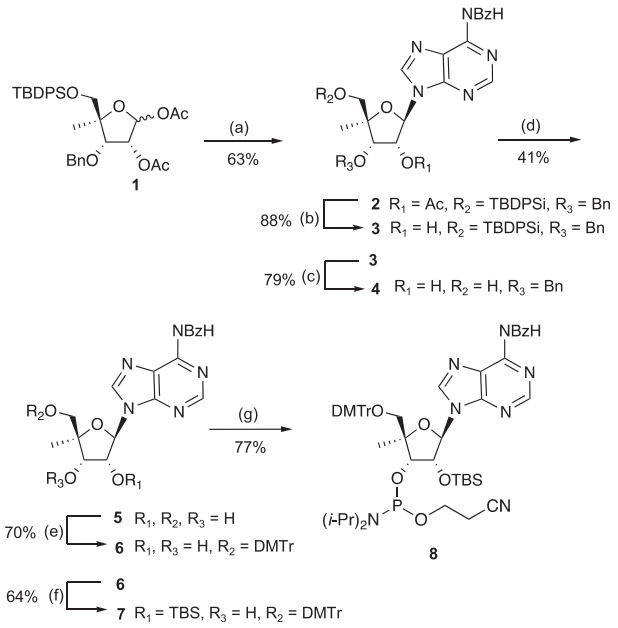


**Scheme 1.** Synthesis of the 4′-*C*-MeA phosphoramidite. Reagents and conditions: (a) $SnCl_4$, $N^6$-benzoyladenine, $CH_2Cl_2$, 0–25°C, 63%; (b) $K_2CO_3$, MeOH, 25°C, 88%; (c) 1 M Tetrabutylammonium fluoride/THF, 25°C, 79%; (d) 1M $BCl_3/CH_2Cl_2$, −78°C, 41%; (e) DMTr-Cl, pyridine, DMAP, 25°C, 70%; (f) *t*-Bu(Me)$_2$Si-Cl, pyridine, $AgNO_3$, THF, 0–25°C, 64%; (g) 2-cyanoethyl-*N,N*-diisopropylchlorophosphoramidite, (*i*-Pr)$_2$NEt, 25°C, 77%.

glycosylations employing Friedel-Craft catalysts, such as $SnCl_4$ (32). Subsequent deacylation of the 2′-OH without the removal of the $N^6$-benzoyl group was accomplished with potassium carbonate ($K_2CO_3$) and methanol in high yields, followed by the desilylation of the 5′-OH with 1M tetrabutylammonium fluoride (TBAF). Debenzylation of the 3′-OH was achieved by employing 1M boron trichloride ($BCl_3$) in $CH_2Cl_2$ to afford **5** in a form ready for advancement to the phosphoramidite. Hence, tritylation of the 5′-OH with *4′4′*-dimethoxytrityl chloride (DMTr-Cl) and pyridine, followed by the regioselective silylation of the 2′-OH in the presence of silver nitrate ($AgNO_3$), pyridine, and *tert*-butyldimethylsilyl chloride (TBS-Cl) provided compound **7** in good yields. The selective silylation of the 2′-OH in ribonucleoside phosphoramidites often produces low yields due to the poor selectivity between the 2′ and 3′ hydroxyl groups (33) However, here we propose that the 2′-silylation reaction furnishes higher than usual yields and selectivity due to the inhibitory/steric effect of the 4′-C methyl group for the 3′-*O*-silylation. The desired isomer was identified by NMR homonuclear correlation of the 1′-2′ protons and one distinct signal from the $^{29}$Si HMBC correlation of the 2′-OSiTBDM–2′-H (Supplementary Information, Figure S1B). Lastly, phosphitylation of the 3′-hydroxyl provided phosphoramidite **8**, suitable for automated RNA synthesis.

## Guide RNAs containing 4′-*C*-MeA at the −1 position do not inhibit ADAR

To test the effect of the sugar modifications at the −1 position, we hybridized chemically modified guide strands to an RNA transcript bearing the sequence from the human methyl CpG binding protein 2 (*MECP2*) containing the W104X site caused by a G-to-A mutation that causes Rett syndrome (34). The resulting duplexes were then allowed to react with purified human ADAR2. The effect of each analog was measured by determining the percent editing at the target site at 60 min (Figure 4A). In addition, the effect of 4′-C-MeA was evaluated by measuring deamination rates under single turnover conditions and compared to duplexes with canonical adenosine (rA) (Figure 4A). We also determined the effect of these analogs in an ADAR1 reaction using a target RNA bearing the mouse *IDUA* W392X nonsense mutation and purified human ADAR1 p110 (Figure 4B). Mutations within the human *IDUA* gene, which encodes α-L-iduronidase, can cause Hurler syndrome (35). The mouse *IDUA* W392X mutation mimics the Hurler-causing human W402X mutation that can be reversed by ADAR-mediated editing and is known to be a good substrate for ADAR1 p110 (20). The effects of having 2′-*O*-MeA, 4′-*C*-MeA, LNA A, and UNA A at the -1 position for ADAR2 and ADAR1 p110 editing are shown in Figure 4. Interestingly, 2′-*O*-MeA and 4′-*C*-MeA behaved similarly to rA and do not show any significant difference in the level of ADAR2 editing at 60 min. Yet, as previously shown by Brinkman et. al, having LNA A at the -1 position inhibited the ADAR2 at the *MECP2* W104X site (10). However, UNA A does show a significant difference in the level of editing compared to rA. Importantly, we determined the ADAR2 deamination rate constant for the 4′-*C*-MeA-containing guide and found it to be indistinguishable from the adenosine-containing guide (Figure 4A).

## Guide RNAs containing 4′-*C*-MeA at the −2 position inhibit the ADAR reaction

RNA editing experiments analogous to those described above were carried out to examine the impact of 4′-C-MeA on ADAR reactivity when it is placed at the −2 position of the gRNA. First, a modified *MECP2* W104X* transcript was designed and generated where the −2 base 5′ of the target was changed from a cytidine to uracil to base pair with 4′-*C*-MeA. Then, guide RNAs containing rA, LNA A, 2′-*O*-MeA and 4′-*C*-MeA at the −2 position were synthesized. *In vitro* deaminations with purified human ADAR2 were carried out and the effect of each analog was measured by determining the percent editing of the target site at the reaction endpoint at 60 min (Figure 5A). Notably, no editing was detected when 4′-*C*-MeA was positioned −2 relative to the target, suggesting that the methyl group of the 4′-*C*-Me in the −2 sugar does indeed clash with P492 (Figure 5C). Likewise, when LNA A was placed at the −2 position, editing was reduced by 86% when compared to the control (-2 rA), displaying similar editing results to those seen with the c-Src target (Figure 1D). No significant difference was observed when 2′-*O*-MeA was positioned −2 relative to the target A, suggesting that this sugar modification is well tolerated at this position for ADAR editing.

## Effect on ADAR editing of 4′-*C*-MeA at various positions of the gRNA

Our previous experiments focused on highlighting the effect of 4′-*C*-MeA when it is placed at the −1 and −2 positions of the gRNA for the MeCP2 and IDUA targets. However, we sought to define the effect of this analog in another sequence context while also evaluating the effect of modification at other positions relative to an editing site. The A-rich c-Src provides

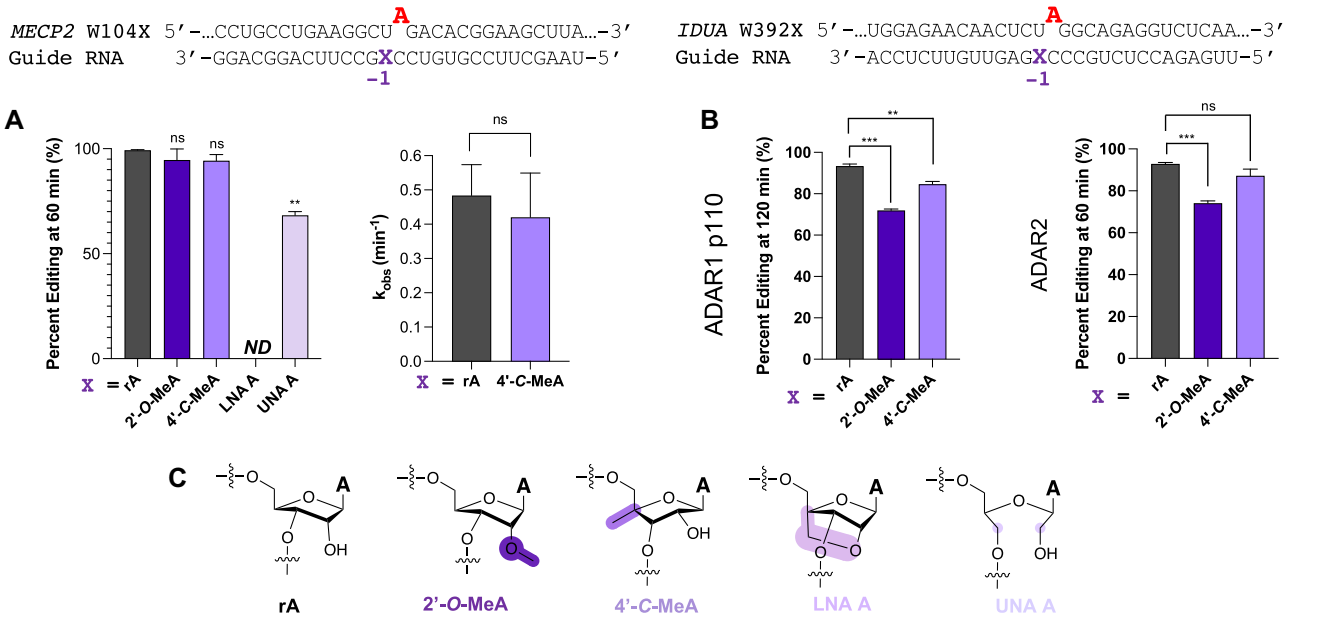


**Figure 4.** (A) Top: Target sequence derived from the mRNA for human *MECP2* proximal to the W104X mutation associated with Rett syndrome and guide RNA used here to direct corrective editing at the premature stop codon. The target adenosine is indicated in red. X indicates the −1 position of the guide strand relative to the target adenosine. Right: Comparison of different ribose modifications at the −1 nucleotide on selective editing at the target site plotted as editing percent at 60 min. Left: Deamination rate comparison of canonical A and 4′-*C*-MeA. Reactions for each timepoint were carried out with a ratio of 5:15 nM of RNA hybrid to ADAR2 WT. (**B**) Top: target sequence derived from the mRNA for mouse *IDUA* proximal to the W392X truncation mutation. Bottom: Effect of different ribose modifications at the −1 nucleotide on ADAR1p110 and ADAR2 WT editing at the target site plotted as editing percent at 120 and 60 min, respectively. Reactions for each timepoint were carried out with a ratio of 15:150 nM of RNA to ADAR1p110 and 5:15 nM for ADAR2 WT. Error bars represent the standard deviation of three technical replicates. A two-tailed Welch's *t* test was conducted, where $*p < 0.05$, $**p < 0.01$, $***p < 0.001$ from rA -1 gRNA; ns: no significant difference. (**C**) Structures of rA, 2′-*O*-MeA, 4′-*C*-MeA, LNA A and UNA A. ND: no detected editing.

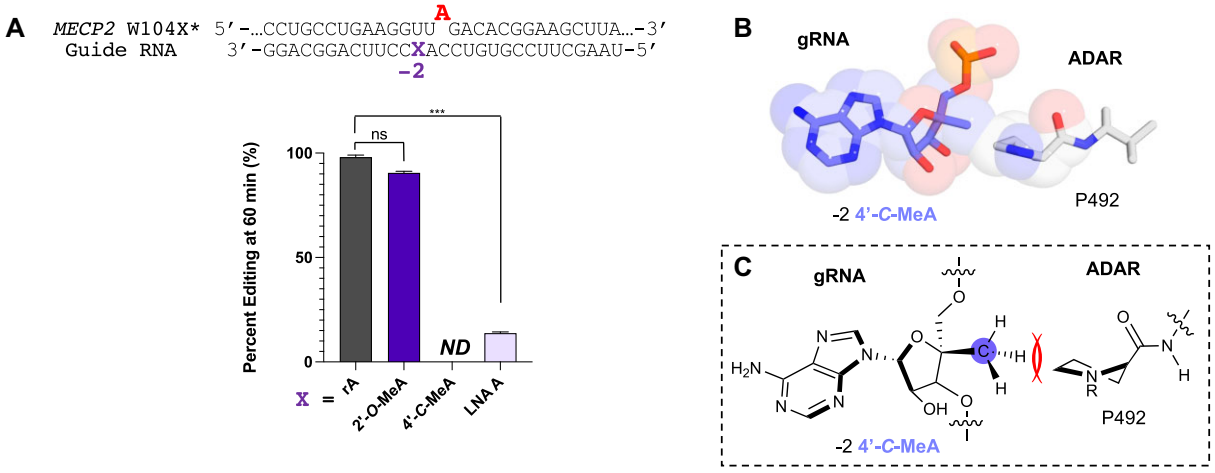


**Figure 5.** (**A**) Comparison of different ribose modifications at the −2 nucleotide on editing at the human modified MECP2* mRNA target site plotted as editing percent at 60 min. Left: reactions for each timepoint were carried out with a ratio of 5:15 nM of RNA hybrid to ADAR2 WT. Error bars represent the standard deviation of three technical replicates. A two-tailed Welch's *t* test was conducted, where $*P < 0.05$, $**P < 0.01$, $***P < 0.001$ from rA -1 gRNA; ns: no significant difference. ND: no detected editing. (**B**) Stick and space-filling model overlay of the −2 4′-*C*-MeA closely approaching the methylene group in Pro 492 of ADAR's flipping loop (19). (**C**) Chemical structure of model of Pro 492 and -2 4′-*C*-MeA in the guide RNA highlighting the location of the predicted steric clash.

a useful framework to achieve this. For this, we placed 4′-*C*-MeA in a gRNA at a position that would be −2 relative to a 5′ adjacent off-target site (blue), −3 relative to the target (red) and −4 and + 1 relative to other bystander sites (grey) (Figure 6A). In vitro deaminations show that 4′-*C*-MeA is still highly inhibitory when placed −2 to the 5′ bystander site, to the point of no detectable editing when compared to a non-modified gRNA (Figure 6A). Interestingly, 4′-*C*-MeA is significantly inhibitory (3-fold reduction in editing level) when placed −3 to the target site. This phenomenon can be attributed to a potential steric clash with ADAR's flipping loop amino acid cluster R481, I456 and F457 and the proximal 4′-C substituent at the −3 nucleotide in the gRNA (Figure 6B). Yet, no significant difference in editing was observed when this analog was placed +1 and −4 relative to other bystander sites.

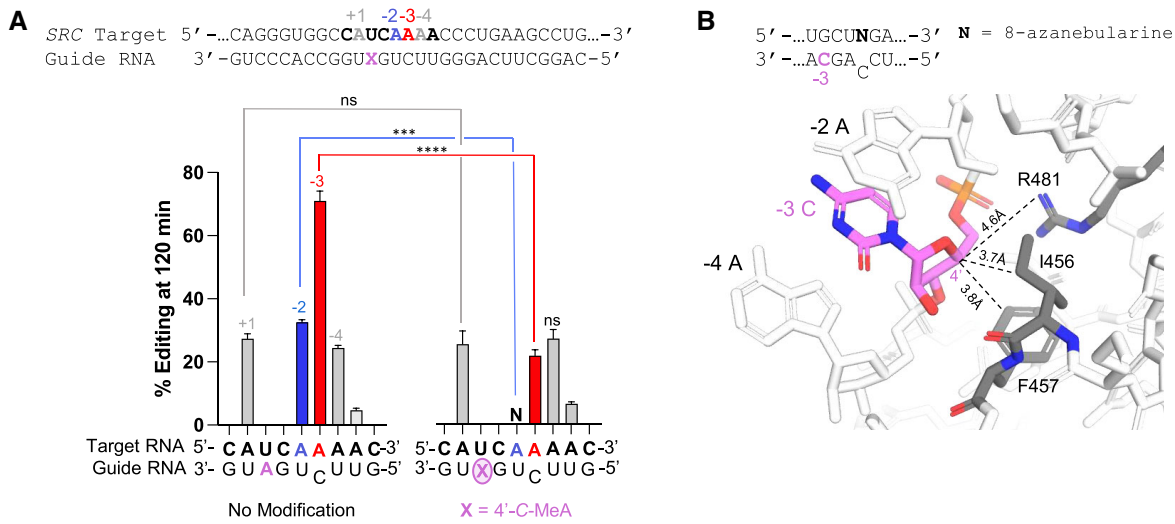


**Figure 6.** Site-specific 4′-*C*-MeA localization in the guide RNA affects ADAR editing of target and proximal off-target sites on the *SRC* transcript. (**A**) Top: schematic of target:guide strand duplex indicating target (red), 5′ adjacent off-target site (blue) and other bystander sites (grey). Guide RNA with X indicating −2 position relative to the 5′ adjacent off-target site (blue), −3 relative to the target (red) and −4 and + 1 relative to other bystander sites. Bottom: ADAR editing yield at 120 min when X = no modification (left) and when X = 4′-*C*-methyladenosine. Red bars indicate editing for target A; −2 off-target site editing is displayed in blue bars and remaining bystander sites editing in grey bars. Reactions for each timepoint were carried out with a ratio of 5:50 nM of RNA hybrid to ADAR2 WT. Error bars represent the standard deviation of three technical replicates. N: No detected editing. (**B**) Structure of hADAR2-R2D E488Q bound to the GLI1 32 bp RNA with 8-azanebularine (N), an ADAR transition state adenosine analog at 2.8 Å resolution; stick model of the -3 nucleotide 4′-*C* closely approaching the side chains of R481, I456 and F457 in ADAR's flipping loop (19).

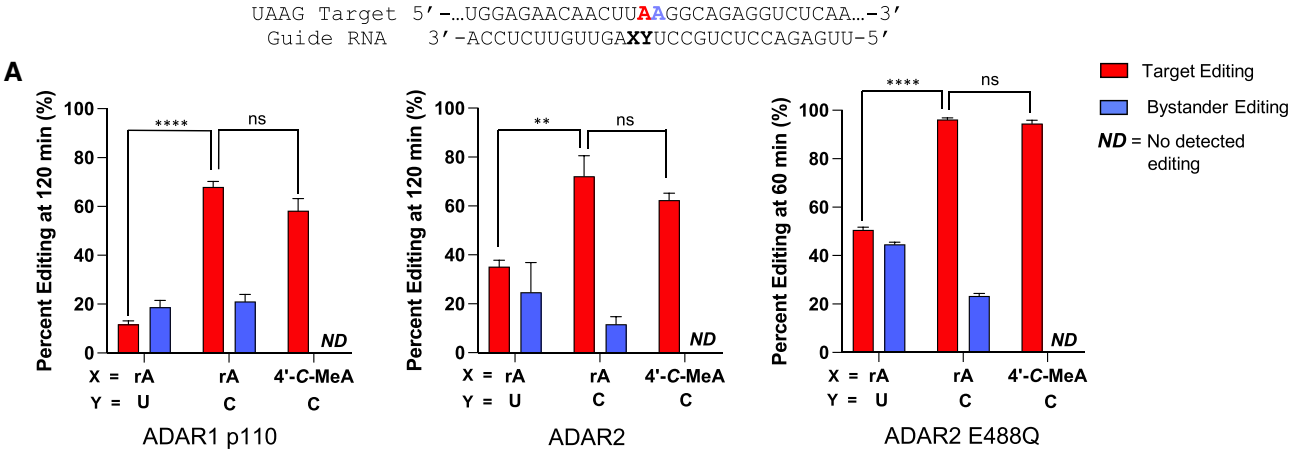


**Figure 7.** Site-specific inhibition of 3′ adjacent bystander editing of the modified mouse IDUA W392X* site (5′-UAA-3′) employing 4′-*C*-methyladenosine (4′-*C*-MeA) modification at the −1 nucleotide with varying orphan bases and ADAR isoforms. (**A**) Top: 5′-UAA-3′ target RNA from modified IDUA with target adenosine (red) and 3′ flanking bystander edit site (blue). X: −1 sugar modification (rA or 4′-*C*-MeA), Y: orphan base (rC or rU). Bottom: ADAR1p110, ADAR2 WT and hyperactive mutant ADAR2 E488Q editing at RNA:enzyme ratios of 15:150, 5:15 and 5:15 nM, respectively. Red bars represent % edited of target A and blue bars % editing of bystander site. Error bars represent the standard deviation of three technical replicates. A two-tailed Welch's *t* test was conducted, where $*P < 0.05$, $**P < 0.01$, $***P < 0.001$; ns: no significant difference. ND: No detected editing.

## 4′-*C*-Me-modified guide RNAs can selectively block adjacent bystander sites while retaining on-target editing efficiency

Since it appeared that 4′-C-methyl modification was tolerated at the −1 position but not at the −2 position of an ADAR guide strand, we decided to test the impact of the modification on a substrate with two adjacent adenosines. Directing ADARs to edit one of two adjacent adenosines can be challenging, particularly if the desired edit is at an adenosine with a non-optimal nearest neighbor nucleotide (36,37). Therefore, we generated a substrate with the target sequence 5′-UAAG-3′, with the desired edit to take place at the first of the two adjacent adenosines and in a non-optimal sequence 5′-UAA-3′ with the adjacent bystander site in the near-optimal 5′-AAG-3′ sequence context. ADAR guide strands were synthesized that vary the nucleotide at the -1 position and orphan position relative to the target adenosine. The duplexes formed with these guide strands were then incubated with human ADAR2 E488Q, a hyperactive mutant of the enzyme or wild-type human ADAR1 p110 (38). Interestingly, with a guide strand of unmodified RNA and uridine at the orphan position (Figure 6AB, X = rA and Y = rU) we find nearly equal editing levels at the two adjacent adenosines with both proteins. With unmodified RNA and cytidine at the orphan position (Figure 6AB, X = rA, Y = rC), the reaction becomes selective for the target A but with significant editing for both ADAR2 E488Q

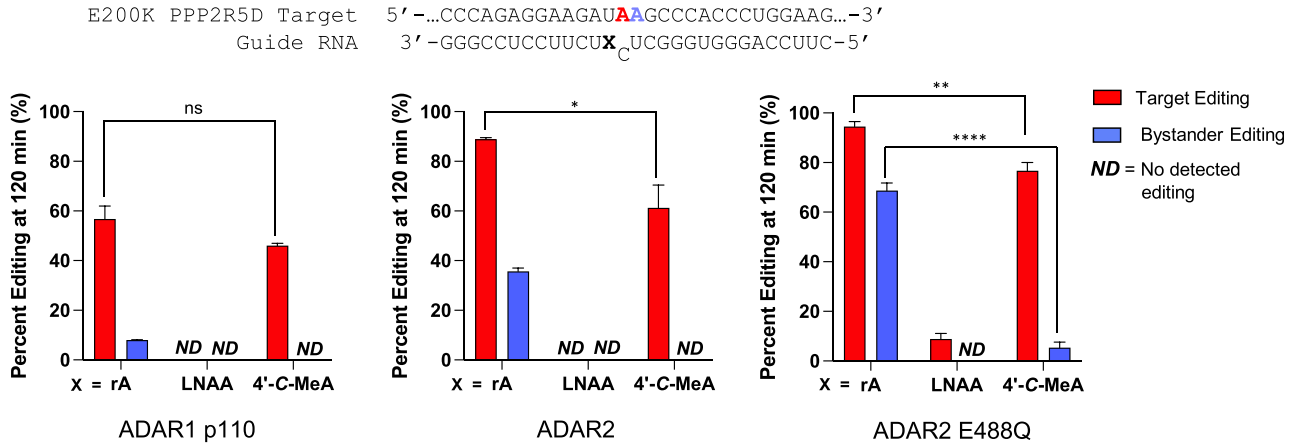


**Figure 8.** Site-specific inhibition of 3′ adjacent bystander editing in a therapeutic transcript employing 4′-*C*-methyladenosine (4′-*C*-MeA) and locked nucleic acid (LNA A). Top: 5′-UAA-3′ target RNA from the human protein phosphatase 2 regulatory subunit B'delta (PPP2R5D) E200K point mutation with the target adenosine (red) and 3′ flanking bystander edit site (blue). X: -1 sugar modification (rA, 4′-*C*-MeA or LNAA). Bottom: ADAR1p110, ADAR2 WT and hyperactive mutant ADAR2 E488Q editing at RNA:enzyme ratios of 5:50 nM at 120 min. Red bars represent % edited of target A and blue bars % editing of bystander site. Error bars represent the standard deviation of three technical replicates. A two-tailed Welch's *t* test was conducted, where $*P < 0.05$, $**P < 0.01$, $***P < 0.001$; ns: no significant difference. ND: No detected editing.

(24 ± 1%) and ADAR1 p110 (21 ± 3%) at the bystander A at the 120 min time point, respectively. However, with both proteins, the guide strand with 4′-*C*-methyladenosine at the −1 position relative to the target site (i.e. −2 position relative to the bystander site) reduces bystander editing to an undetectable level while maintaining efficient editing at the target adenosine (Figure 6AB, X = 4′-C-MeA, Y = rC).

To further evaluate the site-specific inhibitory effect of 4′-modified sugars, we targeted a transcript with a potential therapeutic editing site adjacent to a bystander adenosine (5′-UAAG). Point mutations in the human protein phosphatase 2 regulatory subunit B'delta (*PPP2R5D)* gene can lead to Jordan syndrome, a neurodevelopmental disorder (39). Mutation of the E200 codon of PPP2R5D to a codon for lysine (E200K) is one of the mutations responsible for pathogenic phenotypes in Jordan syndrome patients (40). Reversion of this lysine codon (5′-U *A* ***A***) to glutamic acid (5′-U *G* ***A)*** is expected to restore protein function. Because this site is a 5′-UAAG site, where the target adenosine has a 5′-U neighbor and a 3′-adjacent potential bystander, we generated guide RNAs to stimulate efficient editing at the target site (underlined A), while also blocking undesired editing at the proximal bystander site. To achieve this, we synthesized guide oligonucleotides with A-C mismatches at the target site while placing 4′-*C*-methyladenosine or LNA A at the −2 nucleotide position relative to the bystander site and performed *in vitro* deaminations with three ADAR isoforms (ADAR1p110, ADAR2 and ADAR2 E488Q) (Figure 8). Similar to previous results, we observed that placement of −1 4′-*C*-MeA strongly inhibits the 3′-adjacent bystander site, while retaining substantial on-target editing with all ADAR proteins. Yet, as predicted, LNA A placement −1 to the target inhibits both sites for all ADAR isoforms.

## 4′-*C*-MeA-modified oligonucleotides selectively direct editing in human cells with ADAR2

So far, we have described how selective positioning of 4′-*C*-MeA and LNA A monomers in guide RNAs can block off-targets in biochemical assays with purified ADAR proteins and target RNAs. To determine if the inhibitory effects of these sugars are observed in directed editing experiments in mammalian cells, we synthesized metabolically stable guide oligonucleotides to direct editing by full-length ADAR2 to an endogenous target found in the 3′-UTR of β-actin mRNA (Table S1) (15,41). The guide oligonucleotide was designed to target the 5′-UUAG-3′ sequence where the -1 (X) and -2 (Y) nucleotides in the guide are adenosine analogs. Hence, we tested the effect of having either X or Y = 4′-C-MeA or LNA A, in addition to a control guide with unmodified adenosine as these positions (X, Y = rA) (Figure 9A). Additionally, we stabilized the guide oligonucleotides by replacing most riboses with 2′-*O*-methylriboses and positioning phosphorothioate linkages near the 3′ and 5′ ends, as described previously (Figure 9B) (20,42). Expression of wild-type human ADAR2 in HEK293T cells transfected with the positive control guide (X, Y = rA) led to 30 ± 4% editing at the target site, while the negative control sample (no guide RNA transfection) showed no editing at this site (Figure S4). In the presence of a −1 4′-*C*-MeA guide, a very similar level of 26 ± 1% editing was observed. Yet, when cells were transfected with the −1 LNA A guide, no editing was detected at the target site, indicating complete inhibition by the LNA modification at -1. Inhibition was also observed, albeit to a lesser extent, when the −2 position of the guide was LNA A (3-fold reduction in editing level). Importantly, the guide RNA bearing the 4′-*C*-MeA monomer at the −2 position led to a 4.4-fold reduction in editing level in these experiments, consistent with the inhibition patterns observed in the biochemical assays described above.

## The effects of 4′-*C*-Me A on duplex stability and nuclease sensitivity are similar to adenosine

Lastly, we determined the melting temperature ($T_M$) and ribonuclease sensitivity of RNAs bearing 4′-C-MeA. We conducted thermal denaturation assays to elucidate the impact of 4′-C-MeA on duplex stability and base pairing selectivity. For this purpose, we synthesized 12 nt RNAs containing 4′-C-MeA or adenosine and hybridized them with complementary 12 nt RNAs for $T_M$ measurements (Supplementary Information, Figure S2). The nuclease sensitivity of 4′-C-MeA-containing RNA was assessed using a 15 nt long

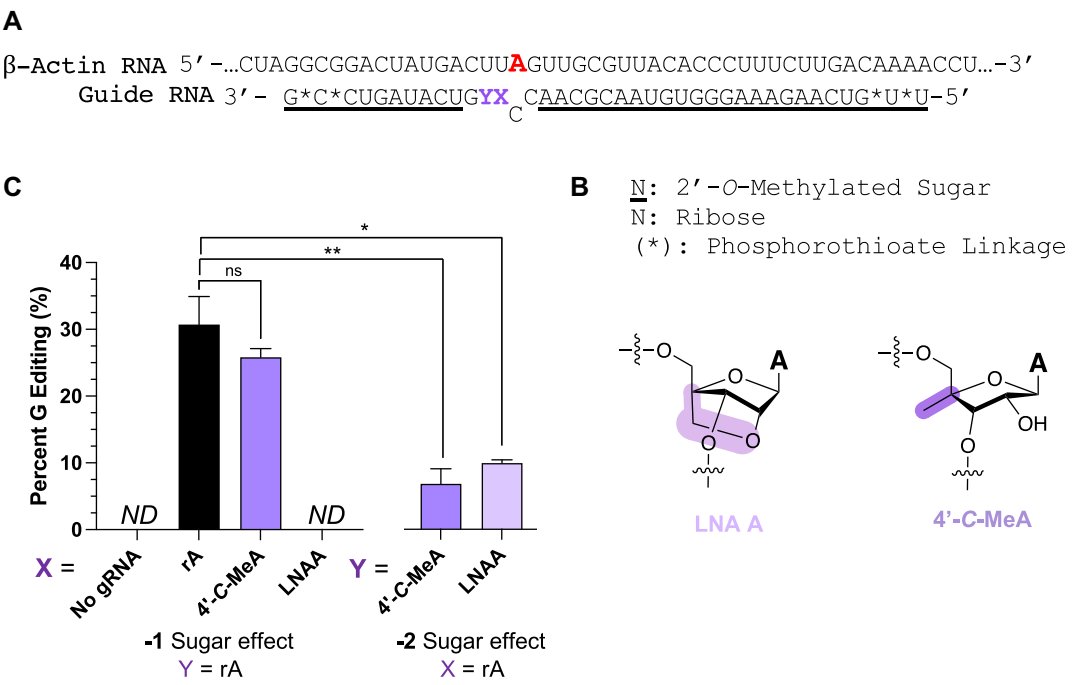


**Figure 9.** Effect of −1 and −2 adenosine analogs in directed editing guide strands targeting an endogenous target in human cells. (**A**) Modification pattern for guide oligonucleotides used in cellular editing and sequence of the endogenous 3′-UTR β-actin transcript and editing site (red) where X (−1) and Y (−2) are modified. (**B**) Structure and denominations of chemical modifications used. (**C**) Percent editing of endogenous β-actin target site in HEK293T cells with overexpressed hADAR2 and varying sugar modifications at the −1 and −2 position of the guide RNA after 48h. Error bars, SD ($n = 3$ biological replicates). ND: no detected editing. A two-tailed Welch's *t* test was conducted, where $*P < 0.05$, $**P < 0.01$, $***P < 0.001$ from rA -1 gRNA; ns: no significant difference.

oligonucleotide with this analog at the 7th position flanked by all 2′-*O*-methyl nucleotides and subjecting it to 80% human serum over a 24 h time course. For comparison, a control oligonucleotide was designed the same, but with rA at the 7$^{th}$ position (Supplementary Information, Figure S3A, B). The $T_M$ analysis showed that 4′-*C*-MeA has an almost identical profile to that of adenosine, suggesting that 4′-methylation of the sugar does not influence the thermal stability of an RNA duplex or pairing selectivity of the nucleobase. However, compared to rA, a slight decrease in serum stability was observed for the 4′-*C*-MeA-containing oligonucleotide.

## Discussion

Oligonucleotide therapeutics is a maturing field with over 15 FDA-approved drugs at the time of this writing (43,44). ADAR-catalyzed therapeutic RNA editing, guided to specific locations in the transcriptome by oligonucleotides, is a novel mechanism of action for oligonucleotide therapeutics (6). Safe and effective drugs that work by this mechanism are currently under development with clinical trials expected to start in 2024 (45,46). ADAR-guiding oligonucleotides for therapeutic RNA editing require extensive modification of the parent RNA to facilitate metabolic stability, cell uptake, and deamination efficiency and selectivity. Several groups have reported efforts in tailoring guide RNAs with chemical modifications (2′-*O*-methyl, 2′-fluoro, phosphorothioate with stereopure backbones, LNA, etc.) for this purpose (7,9,47,48). In this study, we demonstrate the effect of specific sugar-modified nucleotides at different positions in ADAR guide strands varying the proximity to the editing site. Importantly, the effects of different sugar modifications were found to be highly dependent on the position modified and rationalized by analysis of existing ADAR2-RNA crystal structures.

Generally, LNA placement in the guide strand 3′ of the orphan position inhibits editing at the target A. The degree of ADAR inhibition is directly proportional to the proximity of LNA to the editing site. As shown in Figure 1C-E, when LNA is placed between the -4 and -1 positions, the inhibition significantly increases as it approaches the −1 nucleotide. Furthermore, editing of specific adenosines can be entirely inhibited when LNA is placed at either the −1 or −2 positions of the gRNA. In contrast, placing LNA monomers 5′ of the orphan position in the gRNA has substantially less impact on the ADAR reaction. Our previous structural studies showed that the RNA conformation deviates significantly from A-form at the editing site and the adjacent nucleotide on the 5′ side (3′ direction on the guide strand) whereas the RNA conformation 3′ to the editing site is A-form (5′ direction on the guide strand) (21). Thus, the greater severity of ADAR inhibition by LNA substitution on the 3′ side of the guide strand can be explained by the asymmetry of the RNA conformational changes that take place during the ADAR reaction, in addition to the innate rigidity of LNA monomers and their influence on neighboring nucleotides (23,49,50). Lastly, it was observed that LNAs placed at the orphan position render complete inhibition (Figure 1F). This observation is also explained by the inspection of ADAR2-RNA crystal structures. The orphan nucleotide hydrogen bonds with glutamic acid 488 in ADAR2's flipping loop to stabilize the base-flipped conformation while also adopting an unusual sugar pucker that falls in between C2'-*endo* and C3'-*endo* conformations (20). An LNA monomer is likely unable to adopt this conformation and in-

hibits the reaction at this position. Also, if an LNA monomer is located at the position immediately on the 5′ side of the orphan (Figure 1I, +1 LNA), it is likely that the orphan nucleotide will resist the formation of alternate sugar puckers due to the previously reported influence of the vicinal LNA effect (51).

While LNA substitution potently inhibited the ADAR reaction at the −1 and −2 positions of the guide, we found that 4′-*C*-MeA inhibited the ADAR reaction only when placed at position -2. One possible explanation for the lack of inhibition with 4′-*C*-MeA at −1 is that ADAR's I491 side chain may adopt a different conformation to accommodate the 4′-*C*-methyl group emanating from the RNA's minor groove. Interestingly too, based on previous work on the characterization of 4′-*C*-methyluridine monomers in RNA, this type of aliphatic modification promotes a DNA-like C2'-*endo* sugar pucker (28). This structural attribute of the sugar in the 4′-*C*-MeA monomer can be beneficial for ADAR editing when placed at the -1 position based on previous literature that reveals that analogs that favor C2'-*endo* usually promote more efficient deamination than C3'-*endo* nucleotides at this position (10). Based on the biochemical and structural data presented herein, we conclude that LNA monomers positioned at -1 on a gRNA inhibit ADAR by hindering the sugar repuckering required during the ADAR reaction. Finally, it can be inferred that the presence of 4′-*C*-MeA or LNA A at the -2 position leads to inhibition of the ADAR enzyme due to steric clashes, considering that the sugar pucker of the -2 nucleotide does not change upon deamination (Figure 5C). Unlike isoleucine's flexible side chain, proline lacks the conformational flexibility to accommodate the 4′-*C*-Me or methylene bridge emanating from the −2 nucleotide's minor groove of the 4′-*C*-MeA or LNA, respectively. When 4′-*C*-MeA is placed -3 relative to an editing site in the gRNA inhibition is also observed, albeit to a lesser extent (Figure 6A). This can be rationalized by the crystal structures where the −3 nucleotide 4′-carbon is close to a cluster of amino acid side chains (4.6Å–Arg481, 3.7Å–Ile456 and 3.8Å–Phe457).

Considering that the field of therapeutic RNA editing is emergent, there is still a need to regulate bystander editing. The strategic positioning of 4′-*C*-Me monomers in ADAR-guiding oligonucleotides, as described here, is a novel way to achieve this goal. While LNA monomers can block off-target editing at sites that are distal to the target site (i.e. approximately six nucleotides away surrounding the target), using LNA modification to block adjacent bystander editing in a 5′-AA target sequence will likely cause a substantial loss of efficiency at the target site. Nevertheless, as we have shown here for two different RNA targets, placement of a 4′-*C*-Me monomer at the -1 position relative to the target adenosine in a 5′-AA sequence can eliminate editing at the adjacent bystander adenosine while still maintaining high editing efficiency at the target site (Figures 7–8). Finally, we show that the same patterns of inhibition observed in our biochemical assays are seen in a directed editing experiment using metabolically stabilized guide oligonucleotides and cultured human cells.

These structural observations along with biochemical results hint at further chemical manipulations that can be furnished at the minor groove of −1 and −2 nucleotides in the gRNA for the optimization of more selective site-directed editing systems with ADARs. For instance, bulkier 4′-*C* aliphatic nucleotides can be synthesized, as well as engineered ADARs with I491X and P492X mutants to generate new combinations of shape complementarity (i.e. bump-hole method) between the interface of ADAR's flipping loop and the RNA's minor groove. Such combinations could add to the growing list of directed editing systems capable of highly selective corrections of disease-causing mutations at the RNA level (3,20,34,47,52–54).

In summary, we describe a synthesis of 4′-*C*-MeA phosphoramidite and its use to generate modified ADAR guide strands with novel properties. We found that 4′-*C*-MeA behaves similarly to adenosine with respect to its thermal stability in oligoribonucleotides and is slightly more labile to nucleases. 4′-*C*-MeA-modified guides facilitated identification of the mechanistic origin of inhibition of ADAR using site-specific LNA modification, while also shedding additional light on ADAR's base-flipping mechanism (i.e. illustrating the importance of conformational changes happening at the −1, −2 and orphan nucleotides). ADAR inhibition arises for different reasons depending on the placement of the LNA in the guide oligonucleotides relative to the target. An LNA monomer at the −1 position relative to the target renders no editing due to the inhibition of the re-puckering that the -1 sugar must undertake to stabilize the base-flipped complex. Whereas LNA and 4′-*C*-methyl modification at −2 inhibits ADAR due to steric clash with P492. In conclusion, we have provided a framework that describes guide oligonucleotides with different patterns of chemical modifications containing LNAs and 4′-*C*-Me monomers that can be used to achieve efficient ADAR editing while also blocking editing at bystander sites, including within challenging 5′-AA sequences.

## Data availability

The data underlying this article are available in the article and in its online supplementary material.

## Supplementary data

Supplementary Data are available at NAR Online.

## Acknowledgements

We thank William T. Jewell from the Campus Mass Spectrometer Facilities for troubleshooting and aiding in acquiring MALDI-TOF and HF Orbitrap ESI mass spectra. We thank Derrick C. Kaseman for aiding in developing 2D silicon 29 and phosphorus 31 NMR experiments.

## Funding

National Science Foundation Graduate Research Fellowship Program [165004]; Rett Syndrome Research Trust; National Institute of Health Sciences [R35GM141907]. Funding for open access charge: P.A.B. acknowledges financial support from the National Institutes of Health [R35GM141907]; Rett Syndrome Research Trust.

## Conflict of interest statement

P.A.B. is a consultant, S.A.B. member and holds equity in ProQR Therapeutics and holds equity in Beam Therapeutics, companies developing therapeutic editing technologies.

## References


1. Pullirsch,D. and Jantsch,M.F. (2010) Proteome diversification by adenosine to inosine RNA-editing. *RNA Biol*, **7**, 205–212.
2. Yang,Y., Okada,S. and Sakurai,M. (2021) Adenosine-to-inosine RNA editing in neurological development and disease. *RNA Biol*, **18**, 999–1013.
3. Montiel-Gonzalez,M.F., Diaz Quiroz,J.F. and Rosenthal,J.J.C. (2019) Current strategies for site-directed RNA editing using ADARs. *Methods*, **156**, 16–24.
4. Higuchi,M., Maas,S., Single,F.N., Hartner,J., Rozov,A., Burnashev,N., Feldmeyer,D., Sprengel,R. and Seeburg,P.H. (2000) Point mutation in an AMPA receptor gene rescues lethality in mice deficient in the RNA-editing enzyme ADAR2. *Nature*, **406**, 78–81.
5. Khosravi,H.M. and Jantsch,M.F. (2021) Site-directed RNA editing: recent advances and open challenges. *RNA Biol*, **18**, 41–50.
6. Doherty,E.E. and Beal,P.A. (2022) Oligonucleotide-directed RNA editing in primates. *Mol. Ther.*, **30**, 2117–2119.
7. Merkle,T., Merz,S., Reautschnig,P., Blaha,A., Li,Q., Vogel,P., Wettengel,J., Li,J.B. and Stafforst,T. (2019) Precise RNA editing by recruiting endogenous ADARs with antisense oligonucleotides. *Nat. Biotechnol.*, **37**, 133–138.
8. Booth,B.J., Nourreddine,S., Katrekar,D., Savva,Y., Bose,D., Long,T.J., Huss,D.J. and Mali,P. (2023) RNA editing: Expanding the potential of RNA therapeutics. *Mol. Ther.*, **31**, 1533–1549.
9. Diaz Quiroz,J.F., Ojha,N., Shayhidin,E.E., De Silva,D., Dabney,J., Lancaster,A., Coull,J., Milstein,S., Fraley,A.W., Brown,C.R., *et al.* (2023) Development of a selection assay for small guide RNAs that drive efficient site-directed RNA editing. *Nucleic Acid Res*, **51**, e41.
10. Brinkman,H.F., Jauregui-Matos,V., Mendoza,H.G., Doherty,E.E. and Beal,P.A. (2023) Nucleoside analogs in ADAR guide strands targeting 5′-UA sites. *RSC Chem. Biol.*, **4**, 74–83.
11. Zhou,S., Kern,E.R., Gullen,E., Cheng,Y.-C., Drach,J.C., Tamiya,S., Mitsuya,H. and Zemlicka,J. (2006) 9-{[3-Fluoro-2-(hydroxymethyl)cyclopropylidene]methyl}adenines and -guanines. Synthesis and antiviral activity of all stereoisomers. *J. Med. Chem.*, **49**, 6120–6128.
12. Macbeth,M.R. and Bass,B.L. (2007) Large-scale overexpression and purification of ADARs from Saccharomyces cerevisiae for biophysical and biochemical studies. In: Jonatha,G.M. (ed.) *Method Enzymol*. Elsevier, Vol. **424**, pp. 319–331.
13. Jacobsen,C.S., Salvador,P., Yung,J.F., Kragness,S., Mendoza,H.G., Mandel,G. and Beal,P.A. (2023) Library screening reveals sequence motifs that enable ADAR2 editing at recalcitrant sites. *ACS Chem. Biol.*, **18**, 2188–2199.
14. Mendoza,H.G., Jauregui-Matos,V., Park,S., Pham,K.M. and Beal,P.A. (2023) Selective inhibition of ADAR1 using 8-azanebularine-modified RNA duplexes. *Biochemistry*, **62**, 1376–1387.
15. Monteleone,L.R., Matthews,M.M., Palumbo,C.M., Thomas,J.M., Zheng,Y., Chiang,Y., Fisher,A.J. and Beal,P.A. (2019) A Bump-Hole approach for directed RNA editing. *Cell Chem. Biol.*, **26**, 269–277.
16. Hagedorn,P.H., Persson,R., Funder,E.D., Albæk,N., Diemer,S.L., Hansen,D.J., Møller,M.R., Papargyri,N., Christiansen,H., Hansen,B.R., *et al.* (2018) Locked nucleic acid: modality, diversity, and drug discovery. *Drug Discov.Today*, **23**, 101–114.
17. Ferrando,I.M., Chaerkady,R., Zhong,J., Molina,H., Jacob,H.K.C., Herbst-Robinson,K., Dancy,B.M., Katju,V., Bose,R., Zhang,J., *et al.* (2012) Identification of targets of c-Src tyrosine kinase by chemical complementation and phosphoproteomics. *Mol. Cell. Proteom.*, **11**, 355–369.
18. Xu,W., Doshi,A., Lei,M., Eck,M.J. and Harrison,S.C. (1999) Crystal structures of c-Src reveal features of its autoinhibitory mechanism. *Mol. Cell*, **3**, 629–638.
19. Thuy-Boun,A.S., Thomas,J.M., Grajo,H.L., Palumbo,C.M., Park,S., Nguyen,L.T., Fisher,A.J. and Beal,P.A. (2020) Asymmetric dimerization of adenosine deaminase acting on RNA facilitates substrate recognition. *Nucleic Acid Res*, **48**, 7958–7972.
20. Doherty,E.E., Wilcox,X.E., van Sint Fiet,L., Kemmel,C., Turunen,J.J., Klein,B., Tantillo,D.J., Fisher,A.J. and Beal,P.A. (2021) Rational design of RNA editing guide strands: cytidine analogs at the orphan pPosition. *J. Am. Chem Soc.*, **143**, 6865–6876.
21. Matthews,M.M., Thomas,J.M., Zheng,Y., Tran,K., Phelps,K.J., Scott,A.I., Havel,J., Fisher,A.J. and Beal,P.A. (2016) Structures of human ADAR2 bound to dsRNA reveal base-flipping mechanism and basis for site selectivity. *Nat. Struct. Mol. Biol.*, **23**, 426–433.
22. Fisher,A.J. and Beal,P.A. (2017) Effects of Aicardi-Goutières syndrome mutations predicted from ADAR-RNA structures. *RNA Biol*, **14**, 164–170.
23. Campbell,M.A. and Wengel,J. (2011) Locked vs. unlocked nucleic acids (LNA vs. UNA): contrasting structures work towards common therapeutic goals. *Chem. Soc. Rev.*, **40**, 5680.
24. Waga,T., Nishizaki,T., Miyakawa,I., Ohrui,H. and Meguro,H. (1993) Synthesis of 4′- *C* -Methylnucleosides. *Biosci. Biotechnol. Biochem.*, **57**, 1433–1438.
25. Waga,T., Ohrui,H. and Meguro,H. (1996) Synthesis and biological evaluation of 4′- *C* -methyl nucleosides. *Nucleosides. Nucleotides.*, **15**, 287–304.
26. Koizumi,K., Maeda,Y., Kano,T., Yoshida,H., Sakamoto,T., Yamagishi,K. and Ueno,Y. (2018) Synthesis of 4′-C-aminoalkyl-2′-O-methyl modified RNA and their biological properties. *Bioorg. Med. Chem.*, **26**, 3521–3534.
27. Kano,T., Katsuragi,Y., Maeda,Y. and Ueno,Y. (2018) Synthesis and properties of 4′-C-aminoalkyl-2′-fluoro-modified RNA oligomers. *Bioorg. Med. Chem.*, **26**, 4574–4582.
28. Guo,F., Yue,Z., Trajkovski,M., Zhou,X., Cao,D., Li,Q., Wang,B., Wen,X., Plavec,J., Peng,Q., *et al.* (2018) Effect of ribose conformation on RNA cleavage via internal transesterification. *J. Am. Chem. Soc.*, **140**, 11893–11897.
29. Rangam,G., Rudinger,N.Z., Müller,H.M. and Marx,A. (2005) Synthesis and application of 4′-C-alkylated uridines as probes for uracil-DNA glycosylase. *Synthesis (Stuttg)*, **9**, 1467–1472.
30. Nacro,K., Lee,J., Barchi,J.J., Lewin,N.E., Blumberg,P.M. and Marquez,V.E. (2002) Conformationally constrained analogues of diacylglycerol (DAG). Part 19: asymmetric syntheses of (3R)- and (3S)-3-hydroxy-4,4-disubstituted heptono-1,4-lactones as protein kinase C (PK-C) ligands with increased hydrophilicity. *Tetrahedron*, **58**, 5335–5345.
31. Tranová,L. and Stýskala,J. (2021) Study of the $N^7$ Regioselective Glycosylation of 6-Chloropurine and 2,6-Dichloropurine with Tin and Titanium Tetrachloride. *J. Org. Chem.*, **86**, 13265–13275.
32. Vorbrüggen,H. and Höfle,G. (1981) Nucleoside syntheses, XXIII [1] on the mechanism of nucleoside synthesis. *Chem. Ber.*, **114**, 1256–1268.
33. Somoza,Á. (2008) Protecting groups for RNA synthesis: an increasing need for selective preparative methods. *Chem. Soc. Rev.*, **37**, 2668.
34. Sinnamon,J.R., Kim,S.Y., Corson,G.M., Song,Z., Nakai,H., Adelman,J.P. and Mandel,G. (2017) Site-directed RNA repair of endogenous Mecp2 RNA in neurons. *Proc. Natl. Acad. Sci. U.S.A*, **114**, 9395–9402.
35. Wang,D., Shukla,C., Liu,X., Schoeb,T.R., Clarke,L.A., Bedwell,D.M. and Keeling,K.M. (2010) Characterization of an MPS I-H knock-in mouse that carries a nonsense mutation analogous to the human IDUA-W402X mutation. *Mol. Genet. Metab.*, **99**, 62–71.
36. Vogel,P., Moschref,M., Li,Q., Merkle,T., Selvasaravanan,K.D., Li,J.B. and Stafforst,T. (2018) Efficient and precise editing of endogenous transcripts with SNAP-tagged ADARs. *Nat. Methods*, **15**, 535–538.
37. Vallecillo-Viejo,I.C., Liscovitch-Brauer,N., Montiel-Gonzalez,M.F., Eisenberg,E. and Rosenthal,J.J.C. (2018) Abundant off-target edits from site-directed RNA editing can be reduced by nuclear localization of the editing enzyme. *RNA Biol*, **15**, 104–114.
38. Kuttan,A. and Bass,B.L. (2012) Mechanistic insights into editing-site specificity of ADARs. *Proc. Natl. Acad. Sci. U.S.A*, **109**, 3295–3304.

39. Houge,G., Haesen,D., Vissers,L.E.L.M., Mehta,S., Parker,M.J., Wright,M., Vogt,J., McKee,S., Tolmie,J.L., Cordeiro,N., *et al.* (2015) B56δ-related protein phosphatase 2A dysfunction identified in patients with intellectual disability. *J. Clin. Invest.*, **125**, 3051–3062.
40. Wu,C.G., Balakrishnan,V.K., Merrill,R.A., Parihar,P.S., Konovolov,K., Chen,Y.C., Xu,Z., Wei,H., Sundaresan,R., Cui,Q., *et al.* (2024) B56δ long-disordered arms form a dynamic PP2A regulation interface coupled with global allostery and Jordan's syndrome mutations. *Proc. Natl. Acad. Sci. U.S.A.*, **121**, e2310727120.
41. Wettengel,J., Reautschnig,P., Geisler,S., Kahle,P.J. and Stafforst,T. (2017) Harnessing human ADAR2 for RNA repair - Recoding a PINK1 mutation rescues mitophagy. *Nucleic Acids Res.*, **45**, 2797–2808.
42. Vogel,P., Schneider,M.F., Wettengel,J. and Stafforst,T. (2014) Improving Site-Directed RNA Editing In Vitro and in Cell Culture by Chemical Modification of the GuideRNA. *Angew. Chem. Int. Ed.*, **53**, 6267–6271.
43. Al Musaimi,O., Al Shaer,D., Albericio,F. and de la Torre,B.G. (2023) 2022 FDA TIDES (Peptides and Oligonucleotides) Harvest. *Pharmaceuticals*, **16**, 336.
44. Egli,M. and Manoharan,M. (2023) Chemistry, structure and function of approved oligonucleotide therapeutics. *Nucleic Acid Res*, **51**, 2529–2573.
45. Wave Life Sciences USA, Inc. (2023) In: *Wave Life Sciences Announces Submission of First Clinical Trial Application for WVE-006, the First-Ever RNA Editing Clinical Candidate, and Plans for Upcoming Virtual "R&D Day"*. Cambridge, MA.
46. Sheridan,C. (2023) Shoot the messenger: RNA editing is here. *Nat. Biotechnol.*, **41**, 306–308.
47. Monian,P., Shivalila,C., Lu,G., Shimizu,M., Boulay,D., Bussow,K., Byrne,M., Bezigian,A., Chatterjee,A., Chew,D., *et al.* (2022) Endogenous ADAR-mediated RNA editing in non-human primates using stereopure chemically modified oligonucleotides. *Nat. Biotechnol.*, **40**, 1093–1102.
48. Mendoza,H.G. and Beal,P.A. (2023) Chemical modifications in RNA: elucidating the chemistry of dsRNA-specific adenosine deaminases (ADARs). *Acc. Chem. Res.*, **56**, 2489–2499.
49. Wengel,J., Koshkin,A., Singh,S.K., Nielsen,P., Meldgaard,M., Rajwanshi,V.K., Kumar,R., Skouv,J., Nielsen,C.B., Jacobsen,J.P., *et al.* (1999) Lna (Locked Nucleic Acid). *Nucleosides. Nucleotides.*, **18**, 1365–1370.
50. Langkjær,N., Pasternak,A. and Wengel,J. (2009) UNA (unlocked nucleic acid): a flexible RNA mimic that allows engineering of nucleic acid duplex stability. *Bioorg. Med. Chem.*, **17**, 5420–5425.
51. Petersen,M., Bondensgaard,K., Wengel,J. and Jacobsen,J.P. (2002) Locked nucleic acid (LNA) recognition of RNA: NMR solution structures of LNA:RNA hybrids. *J. Am. Med. Chem.*, **124**, 5974–5982.
52. Reautschnig,P., Wahn,N., Wettengel,J., Schulz,A.E., Latifi,N., Vogel,P., Kang,T.-W., Pfeiffer,L.S., Zarges,C., Naumann,U., *et al.* (2022) CLUSTER guide RNAs enable precise and efficient RNA editing with endogenous ADAR enzymes in vivo. *Nat. Biotechnol.*, **40**, 759–768.
53. Abudayyeh,O.O., Gootenberg,J.S., Essletzbichler,P., Han,S., Joung,J., Belanto,J.J., Verdine,V., Cox,D.B.T., Kellner,M.J., Regev,A., *et al.* (2017) RNA targeting with CRISPR–Cas13. *Nature*, **550**, 280–284.
54. Qu,L., Yi,Z., Zhu,S., Wang,C., Cao,Z., Zhou,Z., Yuan,P., Yu,Y., Tian,F., Liu,Z., *et al.* (2019) Programmable RNA editing by recruiting endogenous ADAR using engineered RNAs. *Nat. Biotechnol.*, **37**, 1059–1069.


**Received:** December 10, 2023. **Revised:** April 12, 2024. **Editorial Decision:** May 11, 2024. **Accepted:** May 26, 2024